An Evaluation of Oceanographic Optical Instruments and Deployment Methodologies

Stanford B. Hooker
NASA Goddard Space Flight Center
Laboratory for Hydrospheric Processes
SeaWiFS Project Code 970.2
Greenbelt, MD 20771

Stephane Maritorena
University of California at Santa Barbara
Institute for Computational Earth System Science
6841 Ellison Hall
Santa Barbara, CA 93106

February 17, 1999 Submitted to J. Atmos. Oceanic Tech.

Abstract

The primary objective of the Sea-viewing, Wide Field-of-view Sensor (SeaWiFS) Project is to produce water-leaving radiances with an uncertainty of 5% in clear-water regions and chlorophyll *a* concentrations within ±35% over the range of 0.05–50 $mg\,m^{-3}$. Any global mission, like SeaWiFS, requires validation data be submitted from a wide variety of investigators which places a significant challenge on quantifying the total uncertainty associated with the *in situ* measurements, because each investigator follows slightly different practices when it comes to implementing all of the steps associated with collecting field data, even those with a prescribed set of protocols. This study uses data from multiple cruises to quantify the uncertainties associated with implementing data collection procedures while utilizing differing in-water optical instruments and deployment methods. A comprehensive approach is undertaken and includes a) the use of a portable light source and in-water intercomparisons to monitor the stability of the field radiometers, b) alternative methods for acquiring reference measurements, and c) different techniques for making in-water profiles. The only system to meet the 5% radiometric objective of the SeaWiFS Project was a free-fall profiler using (relatively inexpensive) modular components, although a more sophisticated (and comparitively expensive) profiler using integral components was very close and only 1% higher. A relatively inexpensive system deployed with a winch and crane was also close, but the ship shadow contamination problem increased the total uncertainty to approximately 6.5%.

1. Introduction

The increased availability of commercial off-the-shelf radiometers over the past 20 years has produced a significant increase in the amount of marine optical measurements conducted during oceanographic cruises. Spectral radiometric measurements of the marine light field are now routinely collected in numerous studies related to primary productivity, bio-optical modeling, and ocean color remote sensing. The Sea-viewing Wide Field-of-view Sensor (SeaWiFS) calibration and validation plan (Hooker and McClain 1999), for example, relies on radiometric measurements made at sea by a diverse community of investigators. One of the long-standing objectives of the SeaWiFS Project is to produce spectral water-leaving radiances, $L_W(\lambda)$, with an uncertainty of 5% (Hooker and Esaias 1993), and the sea-truth measurements are the reference data to which the satellite observations are compared (McClain et al. 1998). The accuracy of the field measurements are, therefore, of crucial importance.

The uncertainties associated with *in situ* optical measurements have various sources, such as, the deployment protocols used in the field, the absolute calibration of the radiometers, the environmental conditions encountered during data collection, the conversion of the light signals to geophysical units in a data processing scheme, and the stability of the radiometers in the harsh environment they are subjected to during transport and use. In recent years, progress has been made in estimating the magnitude of some these uncertainties and in defining procedures for minimizing them. For the SeaWiFS Project, the first step in the process of controlling sources of uncertainty was to convene a workshop to draft the SeaWiFS Ocean Optics Protocols (SOOP). The SOOP adhere to the Joint Global Ocean Flux Study (JGOFS) sampling procedures (Joint Global Ocean Flux Study 1991) and define the standards for optical measurements to be used in SeaWiFS radiometric validation and algorithm development (Mueller and Austin 1992). The SOOP are periodically updated as deficiencies are identified and outstanding issues are resolved (Mueller and Austin 1995). Examples of incomplete (but converging consensus) protocols are those for turbid water and above-surface measurements (including those made from aircraft).

The follow-on steps in controlling uncertainty sources investigated a variety of topics. The SeaWiFS Intercalibration Round-Robin Experiment (SIRREX) activity demonstrated that the uncertainties in the traceability between the spectral irradiance of calibration lamps was approximately 1%, and the intercomparisons of sphere radiance was approximately 1.5% in absolute spectral radiance and 0.3% in stability (Mueller et al. 1996). The SeaWiFS Data Analysis Round-Robin (DARR) showed differences in commonly used data processing methods for determining upwelling radiance and downwelling irradiance immediately below and above the sea surface, $L_u(0^-, \lambda)$ and $E_d(0^+, \lambda)$, respectively, were about 3–4% of the aggregate mean estimate (Siegel et al. 1995). Hooker and Aiken (1998) made

estimates of radiometer stability using the SeaWiFS Quality Monitor (SQM), a portable and stable light source, and showed the stability of their radiance and irradiance sensors in the field during a 36-day deployment was on average to within 1% (although some channels occasionally performed much worse). More recently, Hooker et al. (1999) conducted an extensive field program to intercompare a variety of above- and in-water methods to establish the best protocol for making above-water radiometric measurements.

Each of the activities described above focused on one particular aspect associated with in-water light sensors. The way uncertainties combine or cancel, has never been fully assessed, although, SIRREX-5 made an initial inquiry into this important topic and defined an experimental plan for addressing the issues involved (Johnson et al. 1999). Similarly, the recommended protocols allow the same radiometric quantities to be measured using different in-water deployment methodologies (above-surface measurements are not considered here), but the way they compare in the field is poorly documented.

As part of the SeaWiFS Project calibration and validation activities, the SeaWiFS field program conducted specific experiments to investigate these issues. The experiments took place during several Atlantic Meridional Transect (AMT) cruises on board the Royal Research Ship *James Clark Ross* (JCR) between England and the Falkland Islands. The odd-numbered, southbound cruises sample the boreal autumn and austral spring; while the even-numbered, northbound cruises sample the boreal spring and austral autumn (Aiken and Hooker 1997). Because of the geographic extent of the cruises (more than 100° of latitude and 50° of longitude), the repetitive scheduling of the cruises (two per year lasting more than 30 days each), diversity of the environments encountered (oligotrophic gyres to eutrophic coastal regions), and use of state-of-the-art radiometers (including calibration monitoring with the SQM), the AMT Program has no equivalent in the oceanographic community.

The AMT optical experiments were designed to compare a variety of deployment techniques used to measure $L_u(z,\lambda)$ and $E_d(z,\lambda)$. Mounting the needed light sensors on a frame and deploying the frame with a winch and crane is the most frequently used technique, while tethered, free-fall systems are an increasingly popular method. The irradiance incident at the sea surface (often called the reference or *deck cell* measurement) is usually collected with a sensor installed on the ship's deck, but floating references, either above or below the air–sea interface, are also frequently used. Although there are many differences between optical instruments deployed with crane and winch systems versus free-fall units, the primary differences are related to ship-induced perturbations, wave motion, and time required to perform a cast. Cranes have limited reach, so ship shadow can be a problem, whereas for a free-fall system, the profiler (and possibly the reference) is deployed far from the ship to avoid any ship-induced perturbations

to the light field (shadows, reflections, bubbles, etc.). Because ships are not decoupled from the ocean surface, pitch and roll can increase measurement uncertainties in winch and crane deployments, particularly when a long boom is used. Drifting references are also influenced by surface motion, but engineering solutions and deployment practices can be adopted to reduce this effect. Free-fall profilers are not subject to wave action, but they must be properly trimmed to ensure minimal tilts during descent. Winches and cranes require crew preparation time before operations can commence, and winches have relatively low descent and ascent rates, both of which result in increased time needed to complete a cast and, thus, increased opportunities for environmental perturbations (e.g., clouds). Conversely, the deployment or recovery of a free-fall system generally takes a few minutes and can be conducted with only two people.

Assessing the strengths and weaknesses of these deployment methods in the field using radiometers of different types is not a trivial task. Preliminary to any attempt of identifying the actual source of a possible difference between two sensors, it is necessary to know how the sensors compare to one another under controlled circumstances. In other words, the differences in the absolute response of the sensors when they are exposed to a known light source is required, because this establishes a baseline response for each system which permits the other sources of discrepancies during at-sea experiments to be discerned and quantified. The SQM is designed to perform these comparisons and to monitor the stability of the sensors in the field during the length of a cruise. The latter is particularly important, since an actual difference between two deployment schemes must be resolved from a difference caused by a degradation in the performance of a particular sensor. Of course, an independent evaluation of the stability of the SQM itself is needed, so changes in the SQM emitted flux is not incorrectly ascribed to a sensor's performance.

The study presented here deals with all the above-mentioned sources of uncertainty. In particular, the following objectives are considered :

1. Quantify the level of uncertainty of the SQM during AMT cruises;
2. Measure the stability level of the AMT instruments, so differences in the deployment methodologies can be discerned;
3. Compare the stability monitoring capabilities of the SQM (an expensive device) with a time series of in-water and in-air intercomparisons with a second set of radiometers (a potentially inexpensive alternative);
4. Establish which deployment configuration for a reference buoy that can be floated away from a ship produces the smallest uncertainties;
5. Compare reference measurements made far away from a ship to measurements made on a mast mounted above the ship's main deck;

6. Ascertain if a modular, low-cost (16-bit) profiler is as good as an integral, high-cost (24-bit) profiler; and

7. Compare the quality of the data from free-fall systems and from a winch and crane system.

Because the AMT optical measurements are essentially designed for remote sensing validation activities, this study of issues associated with in-water data collection is based on quantities relevant to the validation process, i.e., $L_W(\lambda)$ and diffuse attenuation coefficients derrived from $E_d(z,\lambda)$ and $L_u(z,\lambda)$ profiles, $K_d(\lambda)$ and $K_u(\lambda)$, respectively. The impact of normalizing radiometric quantities by the incident solar irradiance is also considered.

2. Instruments and Methods

Only the AMT instruments supplied by the SeaWiFS Project are considered here, since their calibration and deployment have always adhered to the recommended protocols, and the SQM has always been used to monitor their performance in the field. All of the radiometric systems, including any spares, were manufactured by Satlantic, Inc. (Halifax, Canada). This commonality in equipment was considered the simplest and most cost-effective way to ensure redundacy (exchanging components during failures), intercalibration (very similar center wavelengths), and intercomparison (all of the instruments report at the same rate and have similar response functions).

The SeaWiFS Project instruments used during the AMT Program include the SeaWiFS Optical Profiling System (SeaOPS), the Low-Cost NASA Environmental Sampling System (LoCNESS), and the SeaWiFS Free-falling Advanced Light Level Sensors (SeaFALLS). The former is deployed from a winch and crane, whereas, the latter two are floated away from the ship and deployed by hand. Both SeaOPS and LoCNESS profilers are modular 7-channel systems, that is, they are built up from (relatively) inexpensive subcomponents that are externally cabled together. SeaFALLS and its associated incident irradiance sensors are integral 13-channel designs that cannot be easily disassembled.

The incident solar irradiance data are provided by three instruments. SeaOPS and LoCNESS are deployed in parallel with a 7-channel in-air irradiance sensor mounted on a mast (a deck cell). SeaFALLS is coupled with the SeaWiFS Square Underwater Reference Frame (SeaSURF), which is comprised of an in-water irradiance sensor suspended below a tethered, square floating frame; and the SeaWiFS Buoyant Optical Surface Sensor (SeaBOSS), which is an in-air irradiance sensor fitted inside a removable buoyant collar, so it can be deployed on a mast (as a deck cell) or as a tethered buoy. Figure 1 shows the at-sea use of the SeaWiFS optical instruments within a simplified radiometric schematic [see Hooker and McClain (1999) for a more complete discussion]. A brief description of the instruments and the way they are deployed is given below.

2.1 SQM

The engineering design and characteristics of the SQM are described by Shaw et al. (1997) and Johnson et al. (1998), so only a brief description is given here. The SQM is a portable and highly stable light source capable of monitoring the stability of radiometers to within 1% in the field (Hooker and Aiken 1998). Although the results presented here are from one lamp assembly, the SQM has two lamp sets with different wattage bulbs resulting in three possible flux level settings. The SQM produces a diffuse and uniform light field and is designed to be flush-mounted to radiance or irradiance sensors with a spectral range from 380–900 nm. A kinematically designed D-shaped collar is used on all devices being tested to ensure they view the same part of the SQM aperture each time they are used. The uniformity of the source is less than 2% over a circular area 15 cm in diameter. An internal heater provides operational stability and decreased warm-up intervals.

To account for changes in the emitted flux, three temperature-controlled photodiodes measure the exit aperture light level: one has a responsivity in the blue part of the spectrum, another in the red part of the spectrum, and the third has a broad-band response. It's important to note the blue detector is the most sensitive to illumination fluctuations, since the minimum flux is in the blue part of the spectrum (i.e., the signal-to-noise ratio, SNR, is the lowest). These data are used to normalize the flux of the source, so the actual change in the responsivity of the field sensor can be determined.

A change in the responsivity of the field sensor is distinguished from a change in the internal detectors through the use of fiducials. Fiducials are nonoperational devices with the same size and shape as the *in situ* radiometers. Three fiducials are used: a white one, a black one, and a black one with a glass face. The latter mimics the reflectivity of the optical surface of a radiance sensor (the glass is the same as that used with the field radiometers), but the other two are designed to be significantly different; together, all three provide a wide range of reflectivities. The time series of a fiducial, as measured by the SQM internal monitors, gives an independent measure of the temporal stability of the SQM light field. The reflective surface of fiducials is carefully maintained, both during its use and when it is not being used. Consequently, the reflective surface remains basically constant over the time period of a field expedition. A field radiometer, by comparison, has a reflective surface that is changing episodically due to the wear and tear of daily use. This change in reflectivity alters the loading of the radiometer on the SQM and is a source of variance for the monitors inside the SQM that are viewing the exit aperture, or the radiometer itself when it is viewing the exit aperture.

2.2 SeaOPS

SeaOPS is composed of an above-water and in-water set of 7-channel light sensors organized within modular subsystems. A conductivity and temperature (CT) probe plus a mini-fluorometer are also part of the SeaOPS system. The in-water optical sensors are a downward-viewing OCR-200 radiance sensor which measures $L_u(z,\lambda)$ and an upward-viewing OCI-200 irradiance sensor which measures $E_d(z,\lambda)$. The above-water unit (also an OCI-200 sensor) measures $E_d(0^+,\lambda)$. An in-water and in-air data unit (both Satlantic DATA-100 modules) receive the analog signals from the light sensors and convert them, through a 16-bit, analog-to-digital (A/D) converter, to RS-485 serial communications. The SeaOPS sensors are capable of detecting light over a four-decade range.

A custom-built profiling frame is used to carry SeaOPS. The positioning of the equipment on the frame was developed with a geometry that ensured the light sensors were in close proximity to one another while preventing the radiance sensor from viewing any part of the support. The narrow geometry of the frame was designed to provide a minimal optical cross section. The field of view of the irradiance sensor is only influenced by the 7 mm winch wire and careful attention was paid to the balance of the frame, even though SeaOPS has tilt and roll sensors. At the start of each cruise, the frame was trimmed with lead weights in air, accounting for the in-water weights of the sensors; final trim checks were carried out *in situ* during the first (test) station. The typical lowering and raising speed of the winch was approximately 20–25cm s^{-1}. For most stations, the sun was kept on the starboard side except during adverse weather conditions. The crane used had about a 10 m reach over the starboard side of the ship. During AMT cruises, the SeaOPS reference was always mounted at the top of a mast sited on top of the port stern gantry mast. The mast was high enough to ensure none of the ship's superstructure shaded the irradiance sensor under most illumination conditions.

2.3 SeaFALLS

SeaFALLS, SeaSURF, and SeaBOSS are integral designs all equipped with (relatively expensive) 13-channel OCI-1000 and OCR-1000 radiometers, which employ 24-bit, A/D converters and gain switching. Each system is capable of detecting light over a seven-decade range. SeaFALLS measures $E_d(z,\lambda)$ and $L_u(z,\lambda$ as it falls through the water column. It is based on a SeaWiFS Profiling Multichannel Radiometer (SPMR) which was modified so it could be used with the SQM without any disassembly. SeaSURF is based on a SeaWiFS Multichannel Surface Reference (SMSR), an in-water irradiance sensor designed to be deployed a fixed distance ($z_0 \approx 30$ cm) below the surface, and it measures $E_d(z_0,\lambda)$, while SeaBOSS is an in-air version of the SMSR and measures $E_d(0^+,\lambda)$. All of the

instruments receive power and send data via a tethered cable. Like SeaOPS, SeaFALLS is fitted with a CT probe and a mini-fluorometer.

SeaFALLS is deployed from the stern of the vessel, and whenever possible, the ship maintains a headway speed of approximately 0.5 kts. The profiling instrument is carefully lowered into the water and slowly released at the surface until it has drifted clear of any possible shadowing effect. When the profiler reaches the desired distance from the stern (usually 30–50 m), it is ready for deployment. Continued effort is made of preventing the telemetry cable from ever coming under tension, since even brief periods of tension on the cable can adversely affect the vertical orientation (tilt) and velocity of the profiler. To ensure this does not occur, the operator always leaves a few coils of cable at the surface. A tangle-free and continuous feed of cable into the water is also needed, so all of the cable (approximately 300 m) is laid out or *flaked* on deck prior to each deployment in such a manner as to minimize any entanglements. The profiler descends at approximately $1\,m\,s^{-1}$ so a relatively deep cast can be acquired very quickly (less than 3 minutes for a 150 m cast)

SeaBOSS, can be mounted on a mast or deployed as a drifting buoy, whereas, SeaSURF is always floated away from the boat using a buoyant frame. Any floating references to be deployed at the same time as SeaFALLS are deployed carefully to keep their cosine collectors dry, and then they are held at no less than 15 m behind the vessel until SeaFALLS is in the correct position for deployment. When the drop command is given, both instruments are released in unison. The reference cable is paid out freely so that minimal tension is placed on the cable which in turn minimizes reference tilts. When SeaFALLS reaches the point of maximum descent (usually the 1% light level), both instruments are pulled back to their original positions, and are ready to be redeployed. Since the profiler and both references can be deployed quickly with only two people, the ship can be stopped when light conditions are optimal. More importantly, because SeaFALLS casts do not last long, they can be timed to coincide with clouds moving clear of the sun.

2.4 LoCNESS

LoCNESS is not a new instrument per se, but instead is built up from the SeaOPS modular components or from spares (Fig. 2). Once assembled, LoCNESS is a free-falling unit that looks and functions very similar to SeaFALLS, and it is deployed in the same fashion. The deck cell data is usually the same as for SeaOPS, although, a separate (spare) reference sensor has been used on some occasions. The principle advantage of LoCNESS is its cost and flexibility; it can be assembled from (relatively) inexpensive components (in comparison to SeaFALLS) and it can

be quickly reconfigured, since the radiometers used are not integral to the design. For example, rather than measure E_d and L_u, a spare OCI-200 can be used in place of the OCR-200 radiometer and LoCNESS can measure E_d and E_u. In addition, a special adapter plate can be used on the nose of the profiler which allows for the mounting of two heads rather than one: the usual L_u sensor plus, for example, an E_u sensor. This Three-Headed Optical Recorder (THOR) option does not disturb the stability of the profiler during descent. In fact, the THOR option has produced the lowest and most stable tilts (less than 1° on average) of all the profilers used on AMT cruises.

As shown in Table 1, all of the series 200 radiometers (SeaOPS, LoCNESS) took measurements in the same seven spectral bands which were selected to support SeaWiFS calibration and validation activities (McClain et al. 1992); in comparison, the series 1000 radiometers (SeaFALLS, SeaSURF, and SeaBOSS) cover the SeaWiFS bands plus other parts of the spectrum in greater detail (Table 2). The spectral overlap of the sensors and the simultaneous profiles facilitate at-sea intercomparisons of the instruments. For the analyses presented here, only the SeaWiFS bands are considered, since they are common to all of the instruments.

2.5 Data Acquisition

For all of the profilers, the RS-485 signals from the in-air and in-water subsystems are combined in a Satlantic deck box and converted to RS-232 communications for computer logging. Although the instrument manufacturer provides data acquisition software, it is not suitable for controlling several instruments simultaneously with only one operator, nor is it well suited for calibration monitoring requirements. Consequently, a joint effort was undertaken by the University of Miami Rosenstiel School for Marine and Atmospheric Science (RSMAS) and the SeaWiFS Project to produce a new data acquisition package for all of the AMT optical instruments.

The acquisition software for SeaOPS and LoCNESS is called Combined Operations (C-OPS) and it controls both the in-air and in-water data streams. The primary task of the software is to integrate the RS-232 outputs from the deck box that handles the power and telemetry to the underwater instruments and to control the logging and display of these data streams as a function of the data collection activity being undertaken: dark data (caps on the radiometers), up cast, down cast, constant depth or *soak* events, calibration monitoring, etc. All of the telemetry channels are displayed in real time and the operator can select from a variety of plotting options to visualize the data being collected.

File naming is handled automatically, so all the operator has to do is choose what data streams are to be recorded and then select the execution mode of the data collection activity. The files are written in ASCII and each tab-

delimited file has a header strutcture that identifies what is recorded in each column, and all data records are time stamped. The acquisition software for SeaFALLS functions are very similarly to C-OPS and is called C-FALLS. The primary difference is that C-FALLS logs two rererence data streams (SeaSURF and SeaBOSS) simultaneously.

Data logging for the SQM involves two computer systems: one for the device under test (DUT) and one for the SQM. With the SQM control software, one computer controls two highly regulated power supplies and acquires five other signals from a multiplexed digital voltmeter (DVM): the three photodiode voltages from inside the SQM and the voltages across two precision $1\,\Omega$ shunt resistors. All of this information is time stamped and writted into a tab-delimited ASCII file. The power supplies and the DVM are controlled over a general purpose interface bus (GPIB), and the program acquiring the DVM signals converts the voltage values across the shunts to current, and adjusts the output of the power supplies to ensure a constant current supply to the lamps.

3. Results

To exploit the passage of the JCR, the AMT Program employs three sampling strategies: a) continuous near-surface (7 m) measurements from pumped sea water, b) towed measurements (5–80 m) using the Undulating Oceanographic Recorder (UOR), and c) daily station measurements of the upper ocean (200 m) made close to local solar noon and then again in the mid-afternoon. Although bio-optical measurements are conducted during all three sampling opportunities, the ones of interest for this study are the *in situ* optical measurements made during the latter. In particular, this includes in-water measurements of $E_d(z,\lambda)$ and $L_u(z,\lambda)$ plus in-air and in-water measurements of solar irradiance, $E_d(0^+,\lambda)$ and $E_d(z_0,\lambda)$, respectively. The experiments described in the following sections were conducted during several cruises and generally in Case-1 waters (Morel and Prieur 1977), with chlorophyll *a* concentrations ranging between $0.03\text{–}8.00\text{mg}\,\text{m}^{-3}$.

Starting with AMT-5 (Aiken et al. 1999) and in parallel with the acquisition of data for SeaWIFS validation, specific experiments were executed to allow the intercomparison of data collected by the different radiometers. A concerted effort was made to deploy two or more systems simultaneously as frequently as possible. For these experiments, the beginning of the cast of all instruments were synchronized using hand-held radios, so all sensors experienced very similar illumination conditions in the first 10–20 m of their casts. The SeaOPS (winched) deployments took the longest to complete (typically 15–20 minutes for the down and up casts), so it was usually possible to make several casts with the free-fall instruments during the course of a single SeaOPS cast. These experiments allow the comparison of winched (SeaOPS) versus free-fall (SeaFALLS and LoCNESS) systems and the intercom-

parison of the two free-fall profilers. The former is a way to assess the influence of ship shadow during the winched measurements, and the latter determines if a low cost profiler (LoCNESS) is an acceptable alternative to a higher cost profiler (SeaFALLS).

Another set of deployments using SeaOPS were also conducted taking advantage that the SeaOPS frame was modified so it could collect data from three light sensors. For these experiments two of the ports were occupied by a constant pair of L_u and E_d sensors while another L_u or E_d sensor was connected to the third port to intercompare with the routine ones. Because with these deployments the heads to be compared are almost exactly at the same depth and very close to one another, they experienced virtually identical conditions. For these experiments, the down cast was used to produce a continuous profile for the SeaWiFS validation data set; during the up cast, the profile was stopped at discrete depths (usually five) for one minute soak periods. The soak measurements comprise the intercomparison data set, which were averaged to limit the influence of experimental perturbations caused by waves and ship motion. In addition, sea- and sky-state digital photographs were taken at the bottom of the SeaOPS down cast or in the middle of a sequence of free-fall profiler deployments.

3.1 Calibration Monitoring

Although the SQM lamp ring was changed after it was commissioned during AMT-3, no lamp changes were made after the start of AMT-4, and up through and including AMT-7. Figure 3 shows the percent deviation of the internal SQM blue detector measurements of the glass fiducial with respect to their individual (cruise) mean values during the AMT-4 through AMT-7 cruises (Figs. 3a–3d, respectively). The data in Fig. 3 was from the first lamp set of the lamp ring (which contains two lamp sets). Only one lamp set was used because of time constraints, multiple flux level measurements with the large number of instruments used in the AMT Program (not all of which were used for this study) was too time consuming. The SQM lamp ring was aged for 48 hours before it was used at the start of AMT-4, but Fig. 3a clearly shows an exponential decay in the emitted light during the first few days of AMT-4. Nonetheless, the AMT-4 data indicates the SQM light flux had a stability to within $\pm 0.79\%$ and the data after the first week shows a stability to within $\pm 0.28\%$.

The stability and behavior of the SQM during AMT-5 was very similar to its performance on AMT-3 when it was first commissioned for field use (Hooker and Aiken 1998): the data indicated a step-wise change in the SQM flux level halfway through the cruise. All three detectors showed the change, and if the three detector signals are averaged together, the emitted flux of the SQM decreased by approximately 0.87%. As was the case during AMT-3,

the change in flux was due to a partial short in one of the bulbs which resulted in a 1.2% decrease in the operating voltage of the lamp. The stability of the SQM during the periods before and after the change in light output, as estimated by one standard deviation (1σ) in the average of the three internal monitor signals, was to within 0.60% and 0.53%, respectively.

During AMT-6, the 1σ values of the red, blue, and white detectors while measuring the glass fiducial were 0.36, 0.46, 0.39%, respectively. The performance of the SQM during AMT-6 was the best out of all the cruises; no lamp anomalies were experienced and the standard deviation in the emitted flux was the lowest ever recorded in the field. The AMT-7 data show a step-wise change halfway through the cruise as was seen during AMT-3 and AMT-5. Although the stability for the entire cruise was very good, to within $\pm$0.43% as measured by the blue detector, the stability improves to $\pm$0.38% and $\pm$0.28% if the cruise is split into a first and second half, respectively.

The internal analysis of SQM stability is corroborated by considering the data from R035, one of the field radiometers used during all of the SQM deployments. The peak in the responsivity of the blue internal detector is very close to 443 nm, so a time series of this channel, shown as the + symbols in Fig. 3, is an independent measure of the stability of the SQM during AMT-4 through AMT-7. The average percent deviation with respect to the mean for this channel was 0.77, 0.97, 0.71, 0.92% for AMT-4 through AMT-7, respectively; the same values derived from the internal blue detector analysis were 0.79, 0.80, 0.46, and 0.43%, respectively. The field radiometer data also show the step-wise changes observed during AMT-3, AMT-5, and AMT-7.

3.2 Instrument Stability

Although the agreement of the 443 nm R035 channel with the SQM internal detector establishes the stability of the R035 radiometer, it is but one radiometric channel out of many. A summary of the stability of the *in situ* radiometers during SQM field sessions is shown in Table 3. The data confirms the general behavior originally reported during the AMT-3 cruise (Hooker and Aiken 1998): the radiance sensors are more stable than the irradiance sensors, and the least stable channels are usually the blue irradiance channels. The averages of the most and least stable OCR-200 radiance channels are 0.11% and 0.51%, respectively; the same values for the OCI-200 channels (which includes the OCI-200 references) are 0.39% and 1.90%, respectively. The OCR-1000 and OCI-1000 instruments show similar performance, although, the OCR-1000 sensors perform worse than the OCR-200 instruments. The averages of the most and least stable OCR-1000 radiance channels are 0.26% and 0.79%, respectively; the same values for the OCI-1000 channels (including the references) are 0.34% and 1.93%, respectively.

The greater instability of the irradiance sensors is expected, because a) the cosine collectors reduce the emitted flux, so the blue portion of the spectrum is comparitively lower, b) irradiance sensors have inherently higher noise (from the higher gain resistors in the detector circuits), and c) the greater sensitivity of irradiance sensors to positioning errors. The greater sensitivity of the OCI-1000 sensors, which have 24-bit A/D units does not change this basic conclusion, although, the in-water (higher gain) OCI-1000 sensors do not show as much sensitivity to the blue part of the spectrum.

3.3 Sensor Intercomparisons

In the following comparisons, only the first five SeaWiFS wavelengths (412, 443, 490, 510, and 555 nm, respectively) are considered. The rationale for this is because a) the blue and green channels are the most important to the algorithm validation process; b) the SNR for wavelengths above 600 nm is relatively low, so data at these wavelengths are noisier; and c) high absorption in the red part of the spectrum means that derivation of at the surface values, e.g., $L_u(0^-, \lambda)$, need very specific extrapolation ranges (shallower and narrower than for shorter wavelengths) which are not accounted for in the data processing scheme.

3.3.1 In-Water Comparisons

For the experiments when SeaOPS was equipped with three heads (Section 2.6), R037 (L_u) and I095 (E_d) were always used for routine profile measurements, while the remaining (spare) port was occupied by either R068 (L_u) or I100 (E_d). Figure 4a shows the overall relationship for the first five SeaWiFS wavelengths between the L_u sensors (R037 vs R068) for over 80 simultaneous collection events at various depths. The level of agreement, as determined by the slope of the reduced major axis linear regression (Ricker 1973, and Press and Teukolsky 1992) line (m) and the coefficient of determination (R^2), is very good with a difference of approximately 1.1% ($m = 0.989$, $R^2 = 0.990$, and $N = 451$).

The individual L_u channels show a wider range of disagreement: 4.4, 2.5, 5.6, 24.9, and 3.3% for 412, 443, 490, 510, and 555 nm, respectively. It's important to note, however, that with the exception of the 510 nm channel, the individual channel data are well distributed with respect to the 1:1 line, i.e., there is little evidence of an overall deterministic difference between the two sensors. The overall $E_d(z)$ comparison (Fig. 4b) is also very good, with a difference of approximately 2.7% ($m = 1.027$, $R^2 = 0.999$, and $N = 404$), but the significant clustering of the data above the 1:1 line indicates the two instruments collected deterministically different data. A comparison of the absolute responses of these two irradiance sensors, as determined by the SQM data, shows I095 measured on average

about 2.1% lower than I100 (for the first five SeaWiFS wavelengths), which accounts for almost all of the difference between these two sensors. The E_d values show better agreement at individual wavelengths than the L_u sensors: within 1% in the best case (443 nm) and within 3.4% in the worst (665 nm).

The results presented above were derived from data collected during the up casts when the SeaOPS frame was stopped for 2–3 minutes at discrete depths. The data from the continuous down casts of the same experiments can also be used to assess how data processing, particularly extrapolations of $L_u(z,\lambda)$ to the surface, impact the comparisons of surface quantites like $L_W(\lambda)$ or remote sensing reflectance, $R_{rs}(\lambda)$. $L_W(\lambda)$ is defined as the upwelling light flux just above the sea surface in the zenith direction. This parameter can be obtained by extrapolating the $L_u(z,\lambda)$ profile to the surface and then accounting for the internal reflection during transmission through the air–sea interface. Such extrapolations are performed over homogeneous shallow portions of the water column, generally between 1 and 2 optical depths thick, chosen (by visual examination of the radiometric, CTD, and fluorescence profiles) not to include noisy data close to the surface.

The $L_W(\lambda)$ values derived from R037 and R068 profiles show trends similar to those observed from the soak measurements and the slopes agree to within 1% (Fig. 4c). It is worth noting that because these two sets of comparisons are not exactly of the same kind [compared to the soak comparisons, the $L_W(\lambda)$ comparisons are for a unique depth at a high energy level and have a lower dynamic range], the way errors propagate with data processing cannot be quantified exactly. It is reasonnable, however, to assume that in the example presented above, the uncertainties in $L_W(\lambda)$ introduced by data processing are on the order of 2%.

3.3.2 In-Air Comparisons

During AMT-7, two OCI-200 sensors (M030 and M035) were deployed as deck cells for SeaOPS; both were sited on the starboard, stern trawl post on the same mast. The duplicate reference data allows for an intercomparison of two in-air sensors under almost identical illumination conditions. Figure 5 shows the intercomparison of the two references for over 82 simultaneous collection events (which occurred during the in-water intercomparison profiles summarized in Fig. 4). The agreement between the sensors, as determined by m and R^2, is very good with an overall difference of approximately 1.1% ($m = 0.989$, $R^2 = 0.979$, and $N = 410$). This is better agreement than the SQM analysis would predict, since the latter showed irradiance sensors have an average agreement of approximately 1.9%.

The explanation lies with the results for each channel which show the individual agreement is more variable, but fortuitously grouped around the 1:1 line. The disagreement for the 412, 443, 490, 510, and 555 nm channels are 7.1,

2.7, 3.8, 0.0, and 2.6%, respectively. A recurring bias is the M035 sensor returns higher values than the M030 sensor for all channels, except the 490 nm channel. More importantly, all of the R^2 values for the regression analyses are equal to or greater than 0.995. The large percentage of variance explained implies the differences are deterministic. Since the two sensors were mounted on the same mast, there is no reason to believe the sensors did not experience identical illumination conditions. The SQM data shows the M035 measurements were on average 2.7% higher than the M030 measurements with individual channel differences of 5.1, 1.9, 3.9, 0.6, 1.9%, respectively, which indicates the most likely explanation of the differences in the two sensors is a difference in calibration.

In order to compare in-air reference data from OCI-200 and OCI-1000 sensors simultaneous data from the LoCNESS deck cell (M030) and SeaBOSS (N046) mounted on a mast were collected during AMT-5 and AMT-6 free-fall profiles. Figure 6a shows the two sensors agreed to within 2.6% ($m = 1.026$, $R^2 = 0.987$, and $N = 405$). Again, compared to the 1.9% agreement in the SQM for irradiance sensors, this is very good agreement. Once again, individual channel differences are apparent, and are well explained by the percent differences in the SQM data. Overall, the M030 sensor measured 2.1% greater than N046, but some channels, like the 510 and 555 nm channel, were as much as 5.0% greater and 0.9% lower, respectively. These differences in calibration account for the majority of the individual variances in the *in situ* intercomparisons.

Some of the reference discrepancies resulted from N046 measuring systematically lower irradiances (compared to M030) for some of the experiments at the end of the AMT-5 cruise. The reason for these random lower measurements is unclear. During the SQM sessions, the absolute response of some of the sensors displayed sudden step-wise increases or decreases of a few percent with respect to the running mean. These anomalies took place during the power-up process and were seen to remain for the duration of the session involved, that is, if the sensor powered up with a higher or lower system response, the system remained anomalously higher or lower for the duration of the SQM session. Because these start-up jumps occurred randomly, it is difficult to assess if they are the cause of the $E_d(0^+, \lambda)$ differences observed in the AMT-5 data. Although all instruments exhibited some form of this behavior, the largest jumps were associated with the 24-bit systems. Several others possible causes were investigated (e.g., excessive heat in the radiometers, illumination geometry, and gain switch), but none were correlated with the anomalies.

3.3.3 Reference Deployments Analysis

In ocean color studies, the incident irradiance data are most frequently collected from in-air sensors mounted on deck, but well clear of the ship's superstructure, or from in-water measurements extrapolated above the surface

(Mueller and Austin 1995). Getting the reference data from an instrument located a few tens of centimeters below the surface and oriented towards zenith is a recent alternative (Waters et al. 1990). This kind of deployment allows possible ship influence to be eliminated from the measurements, since the sensor can be installed on a frame and floated far away from the ship (Fig. 1), but several new factors must be accounted for: increased sensor tilts from wave motion, light focusing effects from waves, and the thickness and content of water above the sensor.

In addition to the deck cell comparisons (Section 3.3.2), several experiments were conducted during AMT-5 to compare the benefits and weaknesses of different types of reference deployment methods. SeaBOSS was used to determine how best to float an in-air sensor away from a ship while keeping it dry and minimizing tilts. Four kinds of reference data are considered here:

1. An in-air deck cell reference mounted on a mast and sited as clear of the ship's superstructure as possible (SeaOPS);
2. An in-air reference equipped with a flotation collar (SeaBOSS);
3. An in-air reference equipped with a flotation collar and a buoyant stabilization frame with bunji *isolation* cords fitted between the frame and the body of the irradiance sensor (SeaBOSS modified); and
4. An in-water reference equipped with a buoyant stabilization frame (SeaSURF).

The first three configurations ensured the irradiance sensor was above the air-water interface, and the last three configurations permitted the reference to be floated away from the boat.

SeaBOSS in-air buoy measurements (N046), with no stabilization frame, were compared to simultaneous SeaOPS deck cell (M030) measurements for 42 collection events (Fig. 6b). The overall difference between the references was approximately 6.4% ($m = 0.936$, $R^2 = 0.983$, and $N = 210$). While the variability of the measurements were higher for the buoy references because of wave motion, the mean measurements from the buoy were consistent with the deck cell measurements. When SeaBOSS was equipped with a stabilization frame, the buoy tilts were reduced resulting in a lower standard deviation in this latter case while sea state was rougher (average, minimum, and maximum angles measured with the two configurations cannot be directly compared because instruments were deployed on different days with different sea state). However, no significant change in agreement between SeaBOSS and the SeaOPS reference was observed.

A detailed example of the differences in reference deployments is available from a case study involving three different references. Figures 7a–7c show simultaneous time series from the SeaOPS deck cell (M030), SeaBOSS as a buoy with no stabilization frame (N046), and SeaSURF (H045), respectively; Fig. 7d shows the mean spectrum for each

type of sensor and the mean extraterrestrial solar irradiance, $F_0(\lambda)$, given by Neckel and Labs (1984). The amount of noise or variability in the data increases from the deck cell, to the buoy, and then to the underwater reference with coefficients of variation (standard deviation divided by the mean) equal to 1.0, 2.4, and 8.2%, respectively. The increase in variance between the deck cell and the buoy is due to the enhanced wave motion experienced by the buoy. The large increase in variance between SeaBOSS and SeaSURF is due to the light focusing effect created by surface waves which occasionally results in $E_d(z_0, \lambda)$ values above $F_0(\lambda)$.

A channel-by-channel comparison between the in-water and in-air references (Fig. 7d) reveals the submerged instrument tended to measure higher levels of light at the shorter wavelength and lower values at the longer wavelengths. This latter observation is explained by the strong absorption above 560 nm caused by the (approximately) 30 cm of water between the surface and the cosine collectors of the radiometer. The higher values at shorter wavelengths may come from a higher frequency of (high energy) light flashes caused by surface effects compared to below-average illumination situations. It may be expected that the same effect would be observed along the whole visible spectrum, but high absorption may attenuate or mask such perturbations at long wavelengths. The influence of the intervening water between the sensor and the surface on the spectral shape of the reference spectrum is also dependent upon the concentration of optically active components (i.e., phytoplankton, dissolved organic matter, non-living particulates, etc.). Because normalization of radiometric quantities generally requires the use of incident irradiance above the surface, this implies that sophisticated corrections or filtering procedures need to be applied to the submerged reference measurements.

The spectral shapes of the three references departed somewhat from that of the mean extraterrestrial solar irradiance spectrum. All three reference sensors showed a marked maximum at 510 nm, but such a maximum would be expected at 490 nm in clear-sky conditions or at least both wavelengths should be closer in value. The SQM data showed the 490 nm channel of the N046 sensor measured anomalously low during the cruise, but for this instrument, the relative values of the wavelengths above 500 nm agreed reasonably well with the mean extraterrestrial solar spectrum; the difference between 510 and 555 nm in M030 and H045 seemed high. Again, these are important issues because reference measurements are used to normalize a variety of quantities in ocean color studies.

3.3.4 Profiler Data Analysis

While Section 3.3.1 described results from in-water sensor comparisons conducted with several sensors mounted on the same frame and using the same data logger, this section documents comparisons where several instruments were

used at the same time. During AMT-5 and subsequent cruises, a concerted effort was made to collect simultaneous casts with two and sometimes three profiling radiometers. The main reason for this redundancy was twofold: a) to be able to resolve whether differences between the *in situ* validation data and the remote sensing data were genuine (if both *in situ* measurements agreed, the remote sensing data was considered suspect), and b) to assess the performance of the different sensor systems with respect to one another.

Since the in-water radiance and irradiance measurements are closely dependent upon the incident solar irradiance, it is better for the comparisons to be based on a) quantities which are minimally affected by variations in the incident light field, or b) measurements that are made very close together in time. During simultaneous casts, hand-held radios were used to ensure the instruments were dropped at the same time (so the beginning of the casts were very close together in space and time). Under these conditions, the comparisons can be made on Water-leaving radiances and diffuse attenuation coefficients

The diffuse attenuation coefficient results from absorption and backscattering within the water column, and it quantifies the spectral decrease in light energy as a function of depth. In the present case, it has been derived for the first five SeaWiFS wavelengths by computing the slope of the regression between depth and log-transformed profiles (natural logs) of $L_u(z,\lambda)$ or $E_d(z,\lambda)$ for the depth range used to extrapolate $L_u(z,\lambda)$ values to the surface. Because the derivation of the best possible $L_W(\lambda)$ values is one of the priorities of the data processing scheme, the depth range used to extrapolate radiometric data is mostly based on the shape of the $L_u(z,\lambda)$ profiles. Consequently, this depth range is not always adequate for extrapolating $E_d(z,\lambda)$ values or for computing $K_d(\lambda)$ values, since irradiance measurements are generally subject to deeper and more intense perturbations (particularly from wave focusing effects) than upwelled radiance data. Consequently, $K_u(\lambda)$ is used here to compare measurements from the various radiometers.

Under most circumstances, and in the absence of experimental or environmental perturbations, $K_d(\lambda)$ and $K_u(\lambda)$ are very similar, since the downwelled and upwelled light fluxes are influenced by the same optically active components. This no longer holds true when one set of measurements is influenced by photons that can be considered as coming from a secondary source (i.e., from other than the sun), e.g., fluorescence or Raman scattering. These perturbations are more frequently seen in $L_u(\lambda)$ measurements, because they represent a significant contribution to the measured signal, while they are masked by the (comparitively) higher ambient light level in shallow $E_d(\lambda)$ measurements. Fluorescence and Raman scattering mostly influence long wavelengths (greater than 555 nm), so the data presented here are minimally affected by them.

3.3.4.1 Free-Fall Intercomparisons

Figure 8 shows the intercomparison of $L_W(\lambda)$ (Fig. 8a) and $K_u(\lambda)$ values (Fig. 8b) between the two free-fall instruments LoCNESS (R036) and SeaFALLS (Q016). The data are from 81 simultaneous profiles collected during the AMT-5 and AMT-6 cruises. The overall agreement between the two profilers is very good with approximately a 3% difference in $L_W(\lambda)$ values (m = 1.032, R^2 = 0.980, and N = 405). The LoCNESS $L_W(\lambda)$ estimates are almost always above the 1:1 line, which implies there is a deterministic difference between the two instruments. A comparison of the LoCNESS and SeaFALLS radiometers with the other radiometers used with the SQM showed the SeaFALLS values were on average 1.8% lower than the other radiance sensors. It's important to note that because of the relatively low light level in the SQM, the SQM analysis is only valid for the high gain setting of SeaFALLS while the measurements involved in the derivation of the $L_W(\lambda)$ values often include data acquired at the low gain setting.

Examination of the individual results for each channel shows the agreement between both free-fall instruments for the first three SeaWiFS channels is 1.8, 4.6, and 3.8%, at 412, 443, and 490 nm, respectively. The slope of the regression for the 510 nm channel comparison is considerably worse, m = 1.26. The weak agreement between the two sets is primarly derived from the AMT-6 data where SeaFALLS yielded $L_W(510)$ values lower than LoCNESS. For the 555 nm channel regression m = 1.136, and this is mostly due to six casts from two different stations conducted in waters dominated by *Synecchococcus*. The reason why these stations are not sensed the same way by the two instruments is not clear. Small-scale variability (within a few meters horizontally and vertically) may be one explanation, and there is some evidence for this in the fluorometer data. If these stations are removed from the analysis, the agreement for 555 nm is closer to 7%.

The overall agreement for $K_u(\lambda)$ values is within approximately 1% (m = 1.012, R^2 = 0.980, and N = 405). All of the first three SeaWiFS wavelengths agree to within less than 2%, while the agreement is about 3% and 6% for the 510 and 555 nm channels, respectively (if the *Synecchococcus* stations are removed, the overall agreement is within 3.5% and all wavelengths agree to within 3% except 412 nm which is about 6%).

3.3.4.2 Winched versus Free-Fall Comparisons

Figure 9 shows the intercomparison of $L_W(\lambda)$ (Fig. 9a) and $K_u(\lambda)$ values (Fig. 9b) between the winched system (SeaOPS) and the two free-fall instruments (LoCNESS and SeaFALLS) from a total of 48 simultaneous casts collected during AMT-5 and AMT-7. Differences between SeaOPS and the free-fall instruments are higher than between the

two free-fall sensors with a 8.7% difference for $L_W(\lambda)$ and 2.8% for $K_u(\lambda)$ (the R^2 values are slightly higher than in the free-fall comparison, but this is primarily due to the higher dynamic range in light levels observed in the winched versus free-fall comparisons).

The overall $L_W(\lambda)$ values derived from SeaOPS data were persistently lower (as compared to the 1:1 line) than those from the free-fall instruments (m = 1.087, R^2 = 0.986, and N = 240). This observation holds true at all wavelengths except 510 nm where the free-fall systems measured lower L_W values. Inconsistencies between the 510 channel of various systems were recurrently noted in the AMT experiments. In most cases, the sensors agreed at the illumination level used during calibration. The 510 nm regressions usually crossed the 1:1 line very close to the calibration point, and the largest differences were at the highest illumination levels (above the flux from the single lamp set used with the SQM). Numerous possible causes for these differences were investigated, but no satisfying answer was discerned, and the manufacturer continues to investigate this issue.

While several factors influence the comparison (calibrations, environmental variability, data processing, etc.), the consistently lower values observed for SeaOPS were most probably caused by ship shadow (Gordon 1985; Voss et al. 1985, and Helliwell et al. 1990). The fact that the difference between SeaOPS and the free-fall systems decreases with increasing wavelengths (slopes decrease from 1.107 at 412 nm to 1.04 at 555 nm) reinforce this assumption (Weir et al. 1995). Even though the SeaOPS frame is deployed using a 10 m long crane, the data suggests the measurements are effected by ship shadow, probably because of the large size of the ship (100 m long and ??? m wide). As illustrated by Weir et al. (1995), upwelling radiances, and consequently $L_W(\lambda)$, are more affected by ship shadow than other apparent optical properties (e.g., irradiance). As explained earlier, the SQM analyses cannot fully confirm these trends, because the flux level in the SQM and in the subsurface measurements are different, however, calibration differences should not account for more than 2–3% of the variability observed in the SeaOPS versus free-falls comparisons.

The comparison of the $K_u(\lambda)$ data (Fig. 9b) shows little differences between the two sets of measurements with an overall slope equal to 0.978 while among wavelengths the slope ranges between 1.001 and 0.97 (except, again, for the 510 nm channel). In earlier ship shadow experiments presented by Voss et al. (1986) and Weir et al. (1995), only small differences were also observed in K_d. The fact the K_u comparison does not show obvious ship shadow effect suggests the shadow of the ship has the same impact over the depth range used to calculate the diffuse attenuation coefficient (typically, 3–15 m), otherwise the K_u values for SeaOPS would be lower than those derived from the free-fall instruments.

4. Discussion and Conclusions

The primary objective of this study was to use the AMT data set to quantify the uncertainties associated with many aspects of optical data collection that have not been completely addressed by previous investigations. In particular, a concerted effort was made to resolve differences between deployment schemes and those caused by a degraded performance or calibration of a particular sensor. The latter involved an extensive time series of calibration monitoring using the SQM.

Quantify the level of uncertainty of the SQM during AMT cruises. An analysis of the complete AMT data set for the SQM (AMT-3 through AMT-7, inclusive) confirms the behavior originally reported for AMT-3 (Hooker and Aiken 1998): the stability of the emitted flux is to within approximately 1% over the course of a 30-day deployment. The SQM is probably the most unique optical instrument deployed on the AMT cruises. In the absence of a portable illumination source, like the SQM, scientists deploying radiometers to the field rely on calibration data obtained, at best, before and after field campaigns, and under most circumstances, rely on annual or biannual calibrations. With this kind of calibration scenario, changes in instrument performance are not monitored during a deployment; a linear fit is applied to the calibrations before and after the cruise to estimate any changes in the field. As shown by Hooker and Aiken (1998), this is frequently an inadequate assumption.

Quantify the level of uncertainty of the AMT instruments, so differences in the deployment methods can be discerned. The OCR-200 series instruments have an overall maximum measurement uncertainty of approximately 0.5%. The OCR-1000 instruments are less stable, with an average maximum uncertainty of approximately 0.8%. Both types of irradiance sensors, OCI-200 and OCI-1000, have a similar overall maximum uncertainty of approximately 1.9%. The former are more stable, but the low amount of blue light emitted by the SQM results in higher uncertainties; the latter are less stable, but the higher sensitivity (24-bit A/D and gain switching) compensates for the low flux in the blue part of the spectrum. A channel-by-channel comparison of the two types of irradiance sensors, shows the OCI-200 instruments are more stable if the 412 nm channel is ignored.

Compare the stability monitoring capabilities of the SQM (an expensive device) with a time series of in-water and in-air intercomparisons with a second set of radiometers (a potentially inexpensive alternative). The in-water sensor intercomparisons conducted during AMT-7 showed an overall difference between the L_u and E_d sensors of about 1.1% and 2.7%, respectively. These values are only about 0.6–0.8% higher than the nominal values determined with the SQM, but it's important to note the variance in the individual channels was usually higher in the intercomparison data set than in the SQM data set (which makes error detection more difficult). For the OCR-200 and OCI-

200 radiometers, for example, the differences in the intercomparison data set ranged from 2.5–5.6% and 1.0–3.4%, respectively. The same ranges for the SQM data set were 0.0–1.1% and 0.2–3.7%, respectively; the comparitively poor performance for the SQM irradiance measurements is due to the low flux in the blue part of the spectrum.

Although the degradation in sensitivity from an intercomparison approach may be acceptable for some applications, the biggest problem is two sensors exposed to an unknown illumination level do not permit a unique determination as to which one is wrong in the event of a (nonextreme) difference between the two—this can only be solved if three radiometers are used, but this is no longer an inexpensive alternative. The SQM does provide this capability, because of its independent set of internal monitors, and the fact that the response of all the sensors can be used to determine the difference between normal and anomalous behavior. In addition, the constant output of the SQM permits additional types of testing that cannot be executed in a variable light field. For example, the SQM data was used repeatedly in this study to establish if the *in situ* differences were consistent with differences in calibration (in magnitude and sign).

Establish which deployment configuration for a reference buoy that can be floated away from a ship produces the smallest uncertainties. The intercomparisons between SeaSURF and SeaBOSS conducted during AMT-5 clearly show the submerged reference produces the lowest quality data, primarily because of the negative effects of wave focusing: the two agreed to within no better than 8%. This was one of the largest differences derived from any of the AMT intercomparison experiments. Although more sophisticated filtering or data processing might produce better results, no extra effort is needed with the other reference methods, so the practice of collecting $E_d(z_0, \lambda)$ data was discontinued after AMT-5.

Determine whether or not reference measurements made far away from a ship are superior to measurements made on a mast mounted on the ship. The experiments with the SeaOPS reference and SeaBOSS show an agreement to within about 6.4%. Although adding a stabilization frame to SeaBOSS reduced sensor tilts, longer data sequences than are normally collected were needed to exploit this advantage. The intercomparisons indicate the location and design of the deck cell measurements on the JCR significantly limit or cancel the influence of the ship's superstructure on the data. It must be kept in mind that the potential influence of the ship on the in-air measurements is dependant upon the design (and color) of the ship itself. In the case of the JCR, high superstructures are relatively remote from the stern which constitutes a favorable condition.

Determine whether a modular, low cost (16-bit) profiler is as good as an integral, high cost (24-bit) profiler. The SQM analysis established the superior stability of the 16-bit radiometric systems. This, plus the advantage of being

able to easily change subsystems in the event of reconfiguration requirements or component failures, makes LoCNESS a appealing alternative to SeaFALLS (benefits associated with SeaFALLS having 13 channels compared to LoCNESS having only 7 are not considered here). The intercomparison of the two showed a deterministic difference with the LoCNESS $L_W(\lambda)$ values almost always about 3% higher than the SeaFALLS values. The SQM data confirmed the SeaFALLS data were on average 1.8% lower at low gain than the other radiance sensors used with the SQM.

Determine whether a free-fall system produces better optical data than a winch and crane system. The intercomparison of the LoCNESS and SeaFALLS profilers established that SeaFALLS returned (about 3%) lower data values than LoCNESS. Since the SQM analysis showed the LoCNESS radiometers had a similar response as the SeaOPS radiometers, the higher values from the free-fall units with respect to the SeaOPS measurements means the SeaOPS instrument measured anomalously low (by about 8%). The lower SeaOPS L_W values were probably caused by the influence of the ship's shadow. Although the ship was oriented to minimize this effect, the length of the boom (10 m) used to deploy SeaOPS was probably insufficient to completely eliminate the problem. Another advantage of the free-fall systems is their ease of deployment and the relatively shorter time they require to perform a cast. This is particularly important, because it means casts can be executed in between cloud passage, and more casts can be done in a particular unit of time. It also means station scheduling can be kept informal with the ship being stopped only when illumination conditions are optimal.

The data sets analyzed here addressed a number of specific issues regarding uncertainties arising from *in situ* optical data collection. Table 4 presents a summary of the quantification of these uncertainties as a function of the various deployment systems. All of the instruments have been used on more than one AMT cruise, most of them were modified in between cruises, and all of them involve multiple subsystems, so the entries represent averages biased towards the maximum (average) uncertainties obtained for each source of uncertainty and each subsystem. The main differences in the levels of uncertainty for each source are in calibration and data collection. The 24-bit systems (SeaFALLS) have demonstrably higher noise, so the calibration entries for these instruments are higher than for the 16-bit systems (SeaOPS and LoCNESS). The data collection uncertainties show the widest range of values with different explanations for each system: SeaFALLS equipped with SeaSURF is the largest because of the problem with wave focusing; SeaOPS and SeaFALLS equipped with SeaBOSS are next largest because of ship shadow contamination for the former and wave motion variance for the latter; LoCNESS and SeaFALLS with a deck cell are the best with minimal uncertainties.

The only system to meet the 5% radiometric objective of the SeaWiFS Project is LoCNESS, although SeaFALLS

with a deck cell is very close and only 1% higher. SeaOPS is also close, but the ship shadow contamination problem increases the total uncertainty to 6.5%. It is worth noting that despite the great deal of care taken in all the facets of *in situ* optical data measurements (calibration, shipping, handling, deployment, data processing, etc.), the present analysis reveals that in the best case, the limit of the acceptable level of uncertainty (5%) has been reached. With slightly less attention to any step of the process, it is likely the total uncertainty would increase beyond an acceptable level.

The Table 4 uncertainty estimates are the result of several kinds of experiments and an extensive set of trials, and although the values are close to the hoped for performance, they are averages, and as averages, they mask an important aspect of the study: individual channels (e.g., the 510 nm channel) may perform significantly worse, but the poor performance was only detected and quantified, because of the substantial effort placed on monitoring and intercomparing the sensors in the field. An individiual investigator deploying to the field with only one profiler and a reference would not be able to duplicate this study, and, thus, could not determine the overall or individual performance of the radiometers—the problems with the 510 nm channel, for example, would remain undetected. An SQM would provide a significant improvement, but multiple flux levels outside the calibration point are needed if a thorough understanding of instrument performance is to be acquired. The SQM can provide three flux levels, but this was not used here, because multiple flux level measurements with the large number of instruments used in the AMT Program was too time consuming. An individual investigator with a small number of sensors would not have this problem.

ACKNOWLEDGMENTS

Many individuals have contributed to the success of various components of the SeaWiFS Field Team activities within the AMT Program, including J-F. Berthon, J. Brown, and C. Dempsey; their dedicated contributions are gratefully acknowledged. The stewardship of the Program and the collection of the optical data has been a high priority for J. Aiken; his diligence and commitment has been essential to the high quality of the optical data collected. The participation of S. Maritorena was supported under USRA contract NAS5–32484. The final preparation of the manuscript benefitted from the editorial and logistical assistance of E. Firestone.

Tables

Table 1. Channel numbers and center wavelengths (in nanometers) for the in-water OCR-200 and OCI-200 radiometers used during AMT cruises. All of the channels have 10 nm bandwidths. The instrument codes are composed of a single letter representing the type of instrument and a two-digit serial number. The instrument types are as follows: I for in-water OCI-200, and R for in-water OCR-200.

Channel	*SeaOPS*						*Spares*		*LoCNESS*	
Number	R021	I029	R068	I100	R037	I095	R035	I040	R036	I050
1	411.1	413.0	412.3	412.3	411.0	412.3	411.1	411.5	411.6	411.3
2	443.6	443.2	442.8	443.1	442.8	442.3	442.9	442.5	442.7	442.5
3	489.5	490.5	490.1	489.9	489.9	489.5	489.9	489.5	489.9	489.3
4	509.2	509.2	510.3	510.1	509.7	510.6	509.7	509.6	510.3	509.1
5	555.4	555.5	555.7	555.0	555.0	554.4	555.0	555.2	554.2	554.8
6	665.7	665.6	664.6	665.2	664.8	665.7	665.5	664.9	665.3	666.0
7	683.2	683.8	683.2	683.3	682.7	683.5	683.7	683.5	682.6	682.9

Table 2. Channel numbers and center wavelengths (in nanometers) for the OCI-200 references and the OCR-100 and OCI-100 radiometers used during AMT cruises. All of the channels have 10 nm bandwidths. The instrument codes are composed of a single letter representing the type of instrument and a two-digit serial number. The instrument types are as follows: H for in-water OCI-1000, M for in-air OCI-200, N for in-air OCI-1000, and Q for in-water OCR-1000. Some of the channels (1, 11, and 13) in the SeaFALLS radiometers were changed after AMT-5. The original set (AMT-3, AMT-4, and AMT-5) are denoted by $Q016^1$ and $H023^1$, and the final set (AMT-6 and AMT-7) by $Q016^2$ and $H023^2$. Two sensors are shown for SeaOPS and LoCNESS as well as SeaSURF, because a spare sensor (M035) was used during AMT-7 with the former, and the H045 sensor replaced H024 before AMT-5 for the latter.

Channel	*SeaFALLS*				*SeaOPS/LoCNESS*		*SeaSURF*		*SeaBOSS*
Number	$Q016^1$	$Q016^2$	$H023^1$	$H023^2$	M030	M035	H024	H045	N046
1	406.1	565.0	405.9	564.3	411.9	412.2	406.3	405.8	406.3
2	411.8	411.8	411.1	411.1	443.0	443.0	411.6	412.0	411.7
3	665.8	665.8	665.9	665.9	489.8	489.6	665.7	665.3	665.9
4	443.0	443.0	442.9	442.9	511.0	511.0	443.9	443.4	443.2
5	470.6	470.6	470.4	470.4	555.5	554.8	469.9	470.2	469.9
6	489.3	489.3	489.2	489.2	665.2	669.5	490.6	490.1	489.9
7	510.4	510.4	511.0	511.0	683.7	682.4	509.5	509.8	510.3
8	531.9	531.9	531.5	531.5			532.6	531.8	531.7
9	554.8	554.8	555.3	555.3			555.2	554.1	554.4
10	590.3	590.3	590.2	590.2			590.0	590.1	590.3
11	669.5	519.8	669.6	519.0			670.5	669.6	669.7
12	683.1	683.1	683.6	683.6			683.6	683.1	683.4
13	700.4	434.3	700.4	435.4			700.6	700.6	700.7

Table 3. A summary of the stability of the radiance and irradiance field radiometers used with each optical system (categorized in part by the number of bits used in the A/D converters) during AMT cruises. For each radiometer, the most stable (left-most entry in range) and the least stable (right-most entry in range) channels are shown as percent deviations with respect to the mean behavior of the channel over the cruise time period. Only the SeaWiFS channels are considered for the analysis, and the nominal center wavelengths for the most and least stable channels are shown in parentheses. Although most of the *in situ* analyses presented in this study are based on AMT-5 through AMT-7, AMT-3 and AMT-4 are shown for completeness (to verify trends and average properties).

System	*Cruise*	*Radiance Sensor*		*Irradiance Sensor*	
SeaOPS (16 bits)	AMT-3	R021	0.16 (490) → 0.40 (555)	I029	0.44 (555) → 2.77 (412)
	AMT-4	R021	0.31 (412) → 1.12 (665)	I029	0.53 (490) → 1.62 (683)
	AMT-5	R021	0.16 (665) → 0.68 (683)	I029	0.48 (490) → 1.14 (683)
	AMT-6	R068	0.05 (555) → 0.19 (412)	I100	0.18 (683) → 1.07 (412)
		R035	0.06 (555) → 0.56 (683)	I040	0.65 (510) → 1.53 (443)
		R037	0.03 (555) → 0.36 (683)	I040	0.65 (510) → 1.53 (443)
	AMT-7	R037	0.10 (490) → 0.50 (683)	I095	0.52 (665) → 3.73 (412)
		R068	0.05 (665) → 0.21 (443)	I100	0.27 (555) → 2.18 (412)
Spares (16 bits)	AMT-3	R035	0.12 (683) → 0.57 (510)	I040	0.33 (665) → 1.82 (412)
	AMT-4	R035	0.12 (490) → 0.78 (683)	I040	0.53 (665) → 1.00 (490)
	AMT-5	R035	0.19 (555) → 0.31 (443)	I040	0.46 (665) → 1.07 (443)
	AMT-6	R035	0.06 (555) → 0.56 (683)	I040	0.65 (510) → 1.53 (443)
	AMT-7	R035	0.04 (555) → 0.39 (683)	I040	0.53 (665) → 2.28 (412)
LoCNESS (16 bits)	AMT-5	R021	0.16 (665) → 0.68 (683)	I029	0.48 (490) → 1.14 (683)
	AMT-6	R037	0.03 (555) → 0.36 (683)	I040	0.65 (510) → 1.53 (443)
	AMT-7	R036	0.08 (555) → 0.51 (683)	I050	0.93 (510) → 2.23 (412)
SeaFALLS (24 bits)	AMT-3	Q016	0.09 (490) → 0.31 (412)	H023	0.17 (665) → 0.63 (412)
	AMT-4	Q016	0.41 (665) → 1.55 (683)	H023	0.29 (510) → 1.10 (412)
	AMT-5	Q016	0.30 (665) → 0.47 (412)	H023	0.27 (665) → 0.96 (555)
	AMT-6	Q016	0.29 (665) → 1.00 (683)	H023	0.45 (665) → 0.64 (443)
	AMT-7	Q016	0.22 (665) → 0.63 (683)	H023	0.35 (665) → 0.96 (443)
References (16 bits)	AMT-3			M030	0.24 (510) → 2.62 (412)
	AMT-4			M030	0.21 (665) → 1.41 (412)
	AMT-5			M030	0.30 (665) → 1.93 (412)
	AMT-6			M030	0.06 (665) → 2.24 (443)
	AMT-7			M030	0.25 (665) → 2.30 (412)
				M035	0.11 (510) → 1.18 (412)
References (24 bits)	AMT-3			H024	0.17 (555) → 0.90 (412)
	AMT-4			H024	0.62 (555) → 1.23 (443)
	AMT-5			H045	0.43 (665) → 0.69 (412)
				N046	0.35 (665) → 4.50 (510)
	AMT-6			N046	0.32 (555) → 7.95 (510)
	AMT-7			N046	0.32 (665) → 1.69 (490)

Table 4. A summary of the quantification of total measurement uncertainties as a function of the various deployment systems used in the AMT Program. The systems are shown with their reference configurations. Only SeaFALLS was used with multiple references: the SeaBOSS configuration is SeaBOSS deployed as a buoy, and the deck cell configuration is SeaBOSS on a mast. The entries are average values corrected for deterministic problems identified in the study, e.g., if the SQM analysis showed a particular sensor had an incorrect calibration, the data collection uncertainty for the sensor was recalculated assuming the corrected calibration. Although uncertainties can fortuitously cancel under some circumstances, the total uncercainty for each system is considered to be the sum of the individual contributions.

Source of Uncertainty	*SeaOPS w/Deck Cell*	*LoCNESS w/Deck Cell*	*SeaFALLS w/SeaSURF*	*SeaFALLS w/SeaBOSS*	*SeaFALLS w/Deck Cell*
Calibration	1.5%	1.5%	2.0%	2.0%	2.0%
Data Processing	2.0	2.0	2.0	2.0	2.0
In Situ Stability	1.0	1.0	1.0	1.0	1.0
Data Collection	2.0	0.5	4.0	2.0	1.0
Total	6.5%	5.0%	9.0%	7.0%	6.0%

Figure Captions

Fig. 1. The optical instruments supplied by the SeaWiFS Project for ocean color remote sensing calibration and validation activities within the AMT Program. The two most important negative environmental effects are clouds and foam. The former are the most troublesome, since they can obstruct the direct solar illumination and thereby produce a complicated light field (as shown in the figure for the SeaBOSS instrument). The typical deployment distances to depth and away from the ship are shown in parantheses for the in-water instruments.

Fig. 2. A schematic showing the conversion of SeaOPS into LoCNESS for AMT-5. The deck box provides the (computer controlled) DC power for all of the sensors and is designed to avoid instrument damage due to improper power-up sequences over varying cable lengths. The SeaOPS frame was modified before AMT-6, so three sensors could be clustered together (the third head connects to the spare third port on the DATA-100); LoCNESS was modified at the same time, so two sensors could be mounted on the nose.

Fig. 3. The percent deviation of the internal SQM blue detector measurements of the glass fiducial with respect to their individual (cruise) mean values during a) AMT-4, b) AMT-5, c) AMT-6, and d) AMT-7. The SQM internal detector values are shown as the open symbols, and the 443 nm channel for radiometer R035 is also shown as the + symbols. The latter are an independent measure of the stability of the SQM during AMT-4 through AMT-7.

Fig. 4. The results of intercomparing individual sensors and data processing on the SeaOPS frame during AMT-7: **a)** $L_u(z,\lambda)$ (R068 and R037), **b)** $E_d(z,\lambda)$ (I100 and I095), **c)** $L_W(\lambda)$ (R068 and R037). The diagonal line is the 1:1 line (if the two sensors were calibrated with no deterministic biases and measured exactly the same illumination field, all of the data would be clustered randomly around the 1:1 line).

Fig. 5. The intercomparison of two deck cell references (M035 and M030) during the in-water intercomparison profiles presented in Fig. 4. The AMT sampling is biased towards collecting data during cloud-free conditions, so there is very little data below $50\,\mu\mathrm{W\,cm^{-2}\,nm^{-1}}$ (which can only be reliably collected during overcast conditions).

Fig. 6. An intercomparison of reference measurements collected during simultaneous profiles: **6a)** the LoCNESS deck cell (M030) and SeaBOSS mounted on a mast as a deck cell (N046), and **b)** the SeaOPS deck cell (M030) and SeaBOSS deployed as an in-air buoy with no stabilization frame (N046).

Fig. 7. A case study involving three different references: **a)** the SeaOPS deck cell (M030), **c)** SeaBOSS as a buoy wtih no stabilization frame (N046), and **c)** SeaSURF (H045). The mean spectrum for each sensor (from the deployment time period) and the mean solar irradiance (Neckel and Labs 1984) corrected for transmission through a standard (clear) atmosphere are shown in **d)**.

Fig. 8. An intercomparison of derived values from simultaneous deployments of LoCNESS (R036) and SeaFALLS (Q016): **a)** $L_W(\lambda)$, and **b)** $K_u(\lambda)$.

Fig. 9. An intercomparison of derived values from simultaneous deployments of the winched system (SeaOPS) and the two free-fall instruments (LoCNESS and SeaFALLS): **a)** $L_W(\lambda)$, and **b)** $K_u(\lambda)$.

REFERENCES

Aiken, J., and S.B. Hooker, 1997: The Atlantic Meridional Transect: Spatially extensive calibration and validation of optical properties and remotely-sensed measurements of ocean color. *Backscatter,* **8,** 8–11.

Aiken, J., D.G. Cummings, S.W. Gibb, N.W. Rees, R. Woodd-Walker, E.M.S. Woodward, J. Woolfenden, S.B. Hooker, J-F. Berthon, C.D. Dempsey, D.J. Suggett, P. Wood, C. Donlon, N. González-Benítez, I. Huskin, M. Quevedo, R. Barciela-Fernandez, C. de Vargas, and C. McKee, 1998: AMT-5 Cruise Report. *NASA Tech. Memo. 1998–206892, Vol. 2,* S.B. Hooker and E.R. Firestone, Eds., NASA Goddard Space Flight Center, Greenbelt, Maryland, 113 pp.

Gordon, H.R., 1985: Ship perturbation of irradiance measurements at sea. 1: Monte Carlo simulations. *Appl. Opt.,* **24,** 4,172–4,182.

Helliwell, W.S., G.N. Sullivan, B. Macdonald, and K.J. Voss, 1990: Ship shadowing: model and data comparisons. *Ocean Optics X,* R.W. Spinrad, Ed., SPIE, 1,302, 55–71.

Hooker, S.B., and W.E. Esaias, 1993: An overview of the SeaWiFS project. *Eos, Trans., Amer. Geophys. Union,* **74,** 241–246

Hooker, S.B., and J. Aiken, 1998: Calibration evaluation and radiometric testing of field radiometers with the SeaWiFS Quality Monitor (SQM). *J. Atmos. Oceanic Tech.,* **15,** 995–1,007.

Hooker, S.B., and C.R. McClain, 1999: A comprehensive plan for the calibration and validation of SeaWiFS data. *Progr. Oceanogr.,* (submitted).

Hooker, S.B., G. Zibordi, G. Lazin, and S. McLean, 1999: The SeaBOARR-98 Field Campaign. *NASA Tech. Memo. 1999–206892, Vol. 3,* S.B. Hooker and E.R. Firestone, Eds., NASA Goddard Space Flight Center, Greenbelt, Maryland, 40 pp.

Johnson, B.C., H.W. Yoon, E.A. Early, A. Thompson, S.B. Hooker, R.E. Eplee, JR., R.A. Barnes, and J.L. Mueller, 1999: The Fifth SeaWiFS Intercalibration Round-Robin Experiment (SIRREX-5), July 1996. *SeaWiFS Postlaunch Technical Report Series,* S.B. HOOKER and E.R. FIRESTONE, editors, NASA Goddard Space Flight Center, Greenbelt, Maryland, (submitted).

Joint Global Ocean Flux Study, 1991: JGOFS Core Measurements Protocols. *JGOFS Report No. 6,* Scientific Committee on Oceanic Research, 40 pp.

McClain, C.R., W.E. Esaias, W. Barnes, B. Guenther, D. Endres, S.B. Hooker, G. Mitchell, and R. Barnes, 1992: Calibration and Validation Plan for SeaWiFS, *NASA Tech. Memo. 104566, Vol. 3,* S.B. Hooker and E.R. Firestone, Eds., NASA

Goddard Space Flight Center, Greenbelt, Maryland, 41 pp.

McClain, C.R., M.L. Cleave, G.C. Feldman, W.W. Gregg, and S.B. Hooker, 1998: Science quality SeaWiFS data for global biosphere research. *Sea Tech.*, **39**, 10–15.

Morel, A., and L. Prieur, 1977: Analysis of variations in ocean color. *Limnol. Oceanogr.*, **22**, 709–722.

Mueller, J.L., and R.W. Austin, 1992: Ocean Optics Protocols for SeaWiFS Validation. *NASA Technical Memorandum 104566, Vol. 5,* S.B. HOOKER and E.R. FIRESTONE, editors, NASA Goddard Space Flight Center, Greenbelt, Maryland, 45 pp.

Mueller, J.L., and R.W. Austin, 1995: Ocean Optics Protocols for SeaWiFS Validation, Revision 1. *NASA Tech. Memo. 104566, Vol. 25,* S.B. Hooker, E.R. Firestone, and J.G. Acker, Eds., NASA Goddard Space Flight Center, Greenbelt, Maryland, 66 pp.

Mueller, J.L., B.C. Johnson, C.L. Cromer, S.B. Hooker, J.T. McLean, and S.F. Biggar, 1996: The third SeaWiFS Intercalibration Round-Robin Experiment, SIRREX-3, September 1994. *NASA Tech. Memo. 104566, Vol. 34,* S.B. Hooker, E.R. Firestone, and J.G. Acker, Eds., NASA Goddard Space Flight Center, Greenbelt, Maryland, 78 pp.

Neckel, H., and D. Labs, 1984: The solar radiation between 3300 and 12500. *Solar Phys.*, **90**, 205–258.

Press, W.H., and S.A. Teukolsky, 1992: Fitting straight line data with errors in both coordinates. *Computes in Physics,* **6,** 274–276.

Ricker, W.E., 1973: Linear regressions in fishery research. *J. Fish. Res. Board of Canada,* **30**, 409–434.

Robins, D.B., A.J. Bale, G.F. Moore, N.W. Rees, S.B. Hooker, C.P. Gallienne, A.G. Westbrook, E. Marañón, W.H. Spooner, and S.R. Laney, 1996: AMT-1 Cruise Report and Preliminary Results. *NASA Tech. Memo.,104566, Vol. 35,* S.B. Hooker and E.R. Firestone, Eds., NASA Goddard Space Flight Center, Greenbelt, Maryland, 87 pp.

Shaw, P.-S., B.C. Johnson, S.B. Hooker, and D. Lynch, 1997: The SeaWiFS Quality Monitor–A portable field calibrator light source. *Proc. SPIE,* **2963,** 772–776.

Siegel, D.A., M.C. O'Brien, J.C. Sorensen, D.A. Konnoff, E.A. Brody, J.L. Mueller, C.O. Davis, W.J. Rhea, and S.B. Hooker, 1995: Results of the SeaWiFS Data Analysis Round-Robin (DARR-94), July 1994. *NASA Tech. Memo. 104566, Vol. 26,* S.B. Hooker and E.R. Firestone, Eds., NASA Goddard Space Flight Center, Greenbelt, Maryland, 58 pp.

Voss, K.J., J.W. Nolten, and G.D. Edwards, 1986: Ship shadow effects on apparent optical properties. *Ocean Optics VIII,* P.N. Platter, Ed., SPIE, 637, 186–190.

Waters, K.J., R.C. Smith, and M.R. Lewis, 1990: Avoiding ship induced light-field perturbation in the determination of oceanic optical properties. Oceanogr., **3**, 18–21.

Weir, C.T., D.A. Siegel, D.W. Menzies, and A.F. Michaels, 1995: *In situ* evaluation of a ship's shadow, *NASA Tech. Memo. 104566, Vol. 27*, S.B. Hooker, E.R. Firestone, and J.G. Acker, Eds., NASA Goddard Space Flight Center, Greenbelt, Maryland, 46 pp.

Figure 1

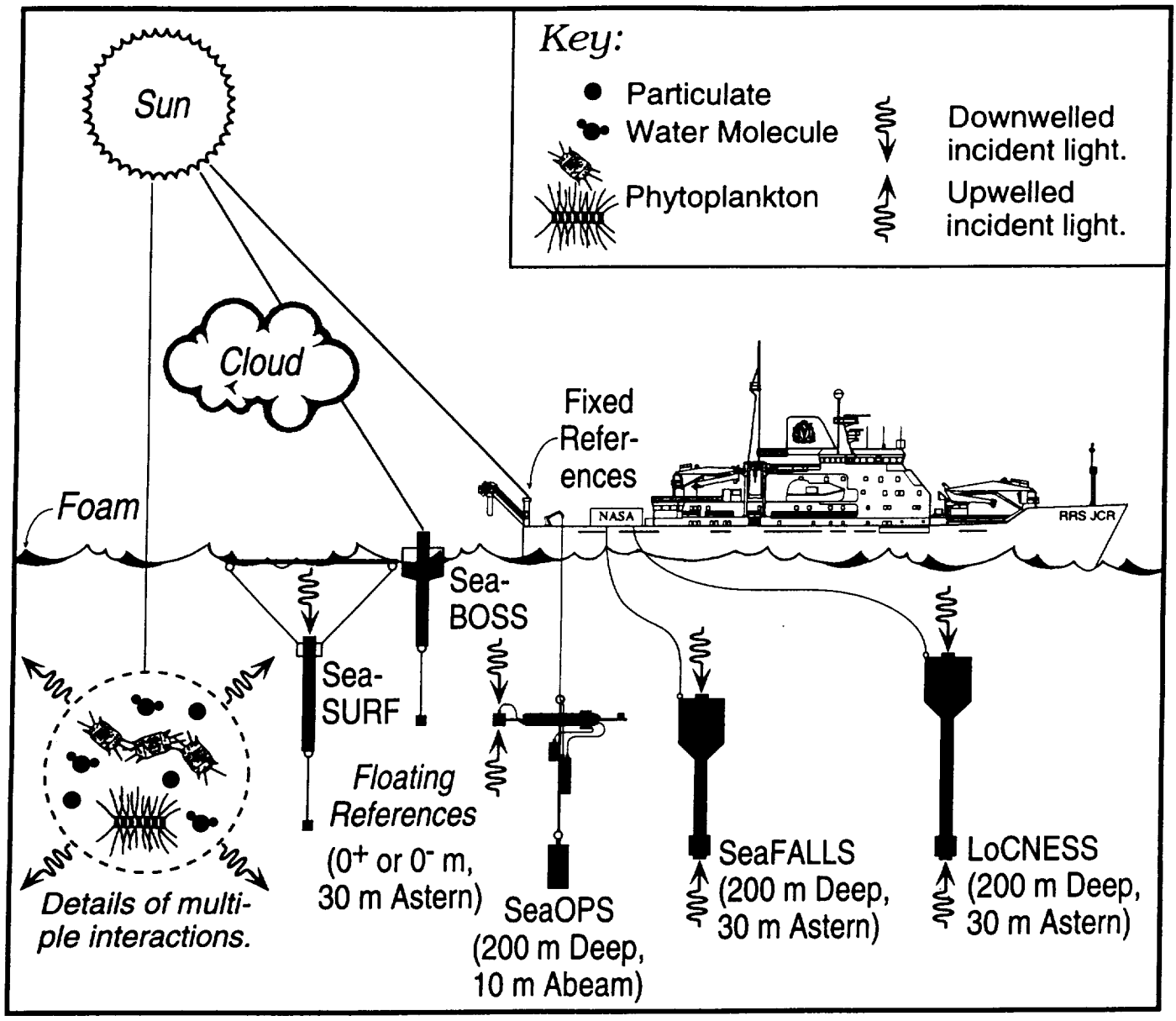
Key:
Particulate
Water Molecule
Phytoplankton
Downwelled incident light.
Upwelled incident light.
Sun
Cloud
Foam
Fixed References
NASA
RRS JCR
Sea-BOSS
Sea-SURF
Floating References
(0+ or 0- m, 30 m Astern)
SeaOPS (200 m Deep, 10 m Abeam)
SeaFALLS (200 m Deep, 30 m Astern)
LoCNESS (200 m Deep, 30 m Astern)
Details of multiple interactions.

Figure 2

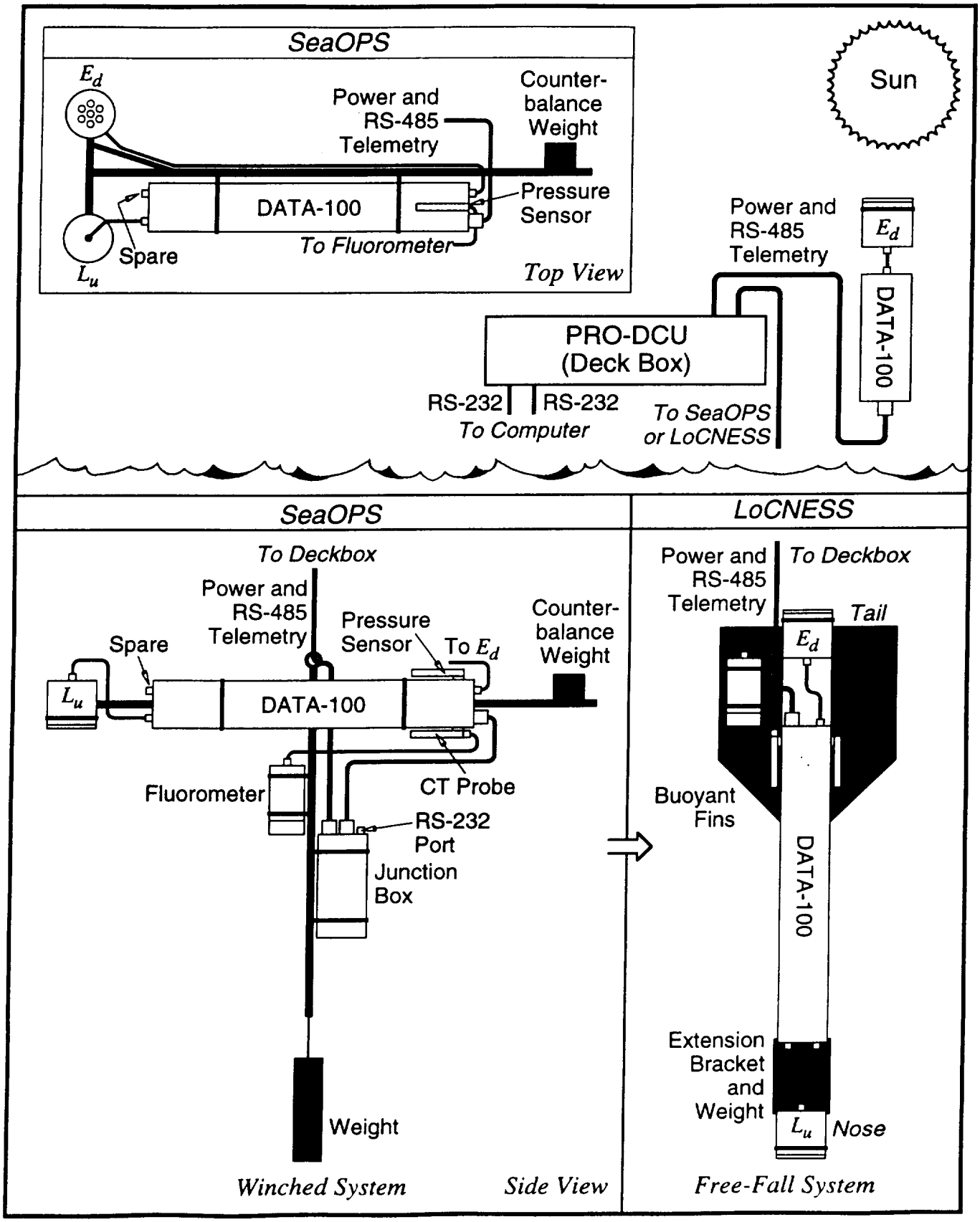
SeaOPS
E_d
Power and RS-485 Telemetry
Counter-balance Weight
DATA-100
Pressure Sensor
To Fluorometer
Spare
L_u
Top View
Sun
Power and RS-485 Telemetry
E_d
DATA-100
PRO-DCU (Deck Box)
RS-232
RS-232
To Computer
To SeaOPS or LoCNESS
SeaOPS
LoCNESS
To Deckbox
Power and RS-485 Telemetry
Pressure Sensor
To E_d
Counter-balance Weight
Spare
L_u
DATA-100
Fluorometer
CT Probe
RS-232 Port
Junction Box
Weight
Winched System
Side View
Power and RS-485 Telemetry
To Deckbox
Tail
E_d
Buoyant Fins
DATA-100
Extension Bracket and Weight
L_u
Nose
Free-Fall System

Figure 3

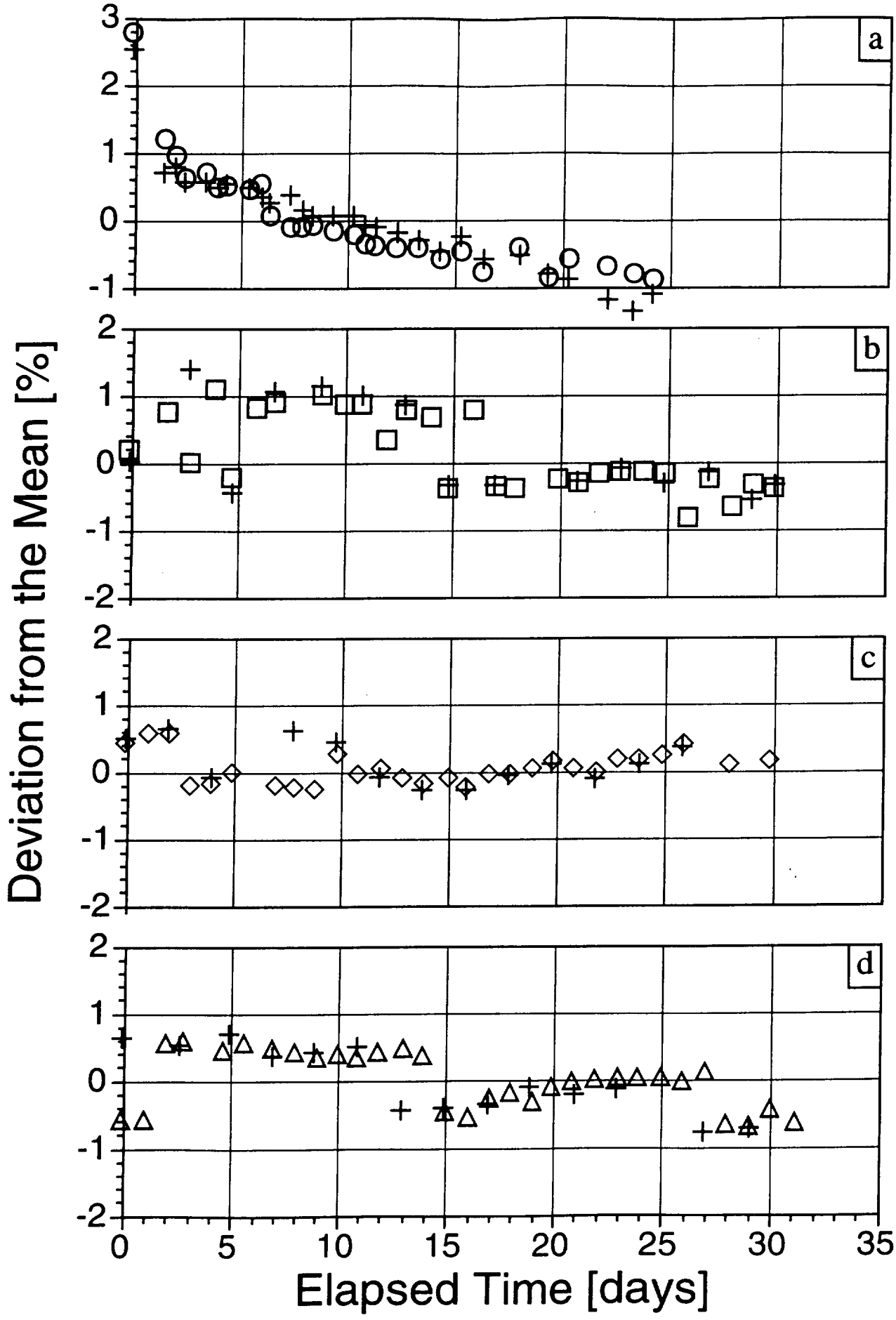
a
b
c
d
Deviation from the Mean [%]
Elapsed Time [days]
3
2
1
0
-1
-2
0
5
10
15
20
25
30
35

Figure 4a

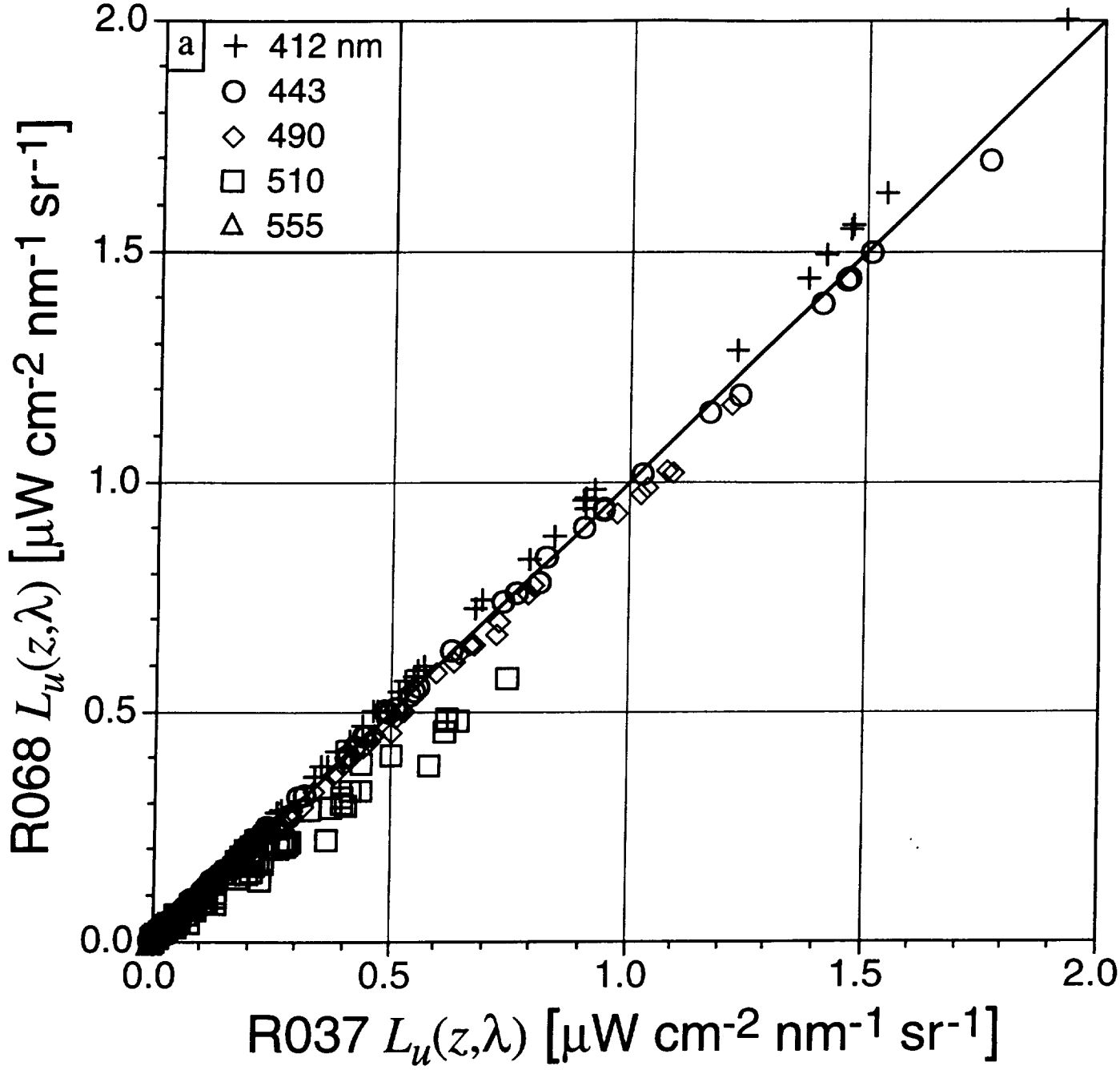
a
412 nm
443
490
510
555
2.0
1.5
1.0
0.5
0.0
0.0
0.5
1.0
1.5
2.0
R068 $L_u(z,\lambda)$ [μW cm^{-2} nm^{-1} sr^{-1}]
R037 $L_u(z,\lambda)$ [μW cm^{-2} nm^{-1} sr^{-1}]

Figure 4l

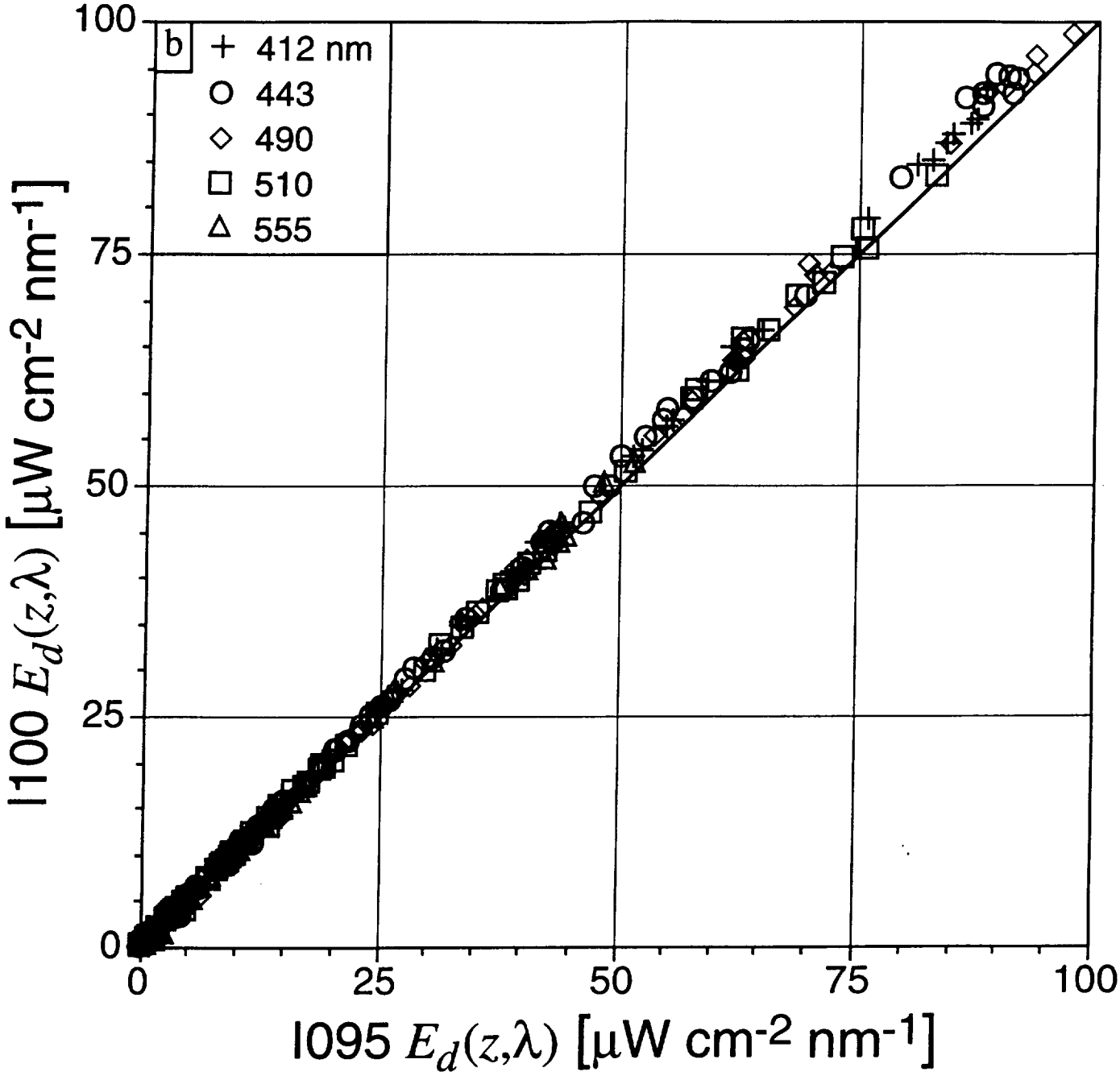
b
412 nm
443
490
510
555
100
75
50
25
0
0
25
50
75
100
l100 $E_d(z,\lambda)$ [μW cm-2 nm-1]
l095 $E_d(z,\lambda)$ [μW cm-2 nm-1]

Figure 4c

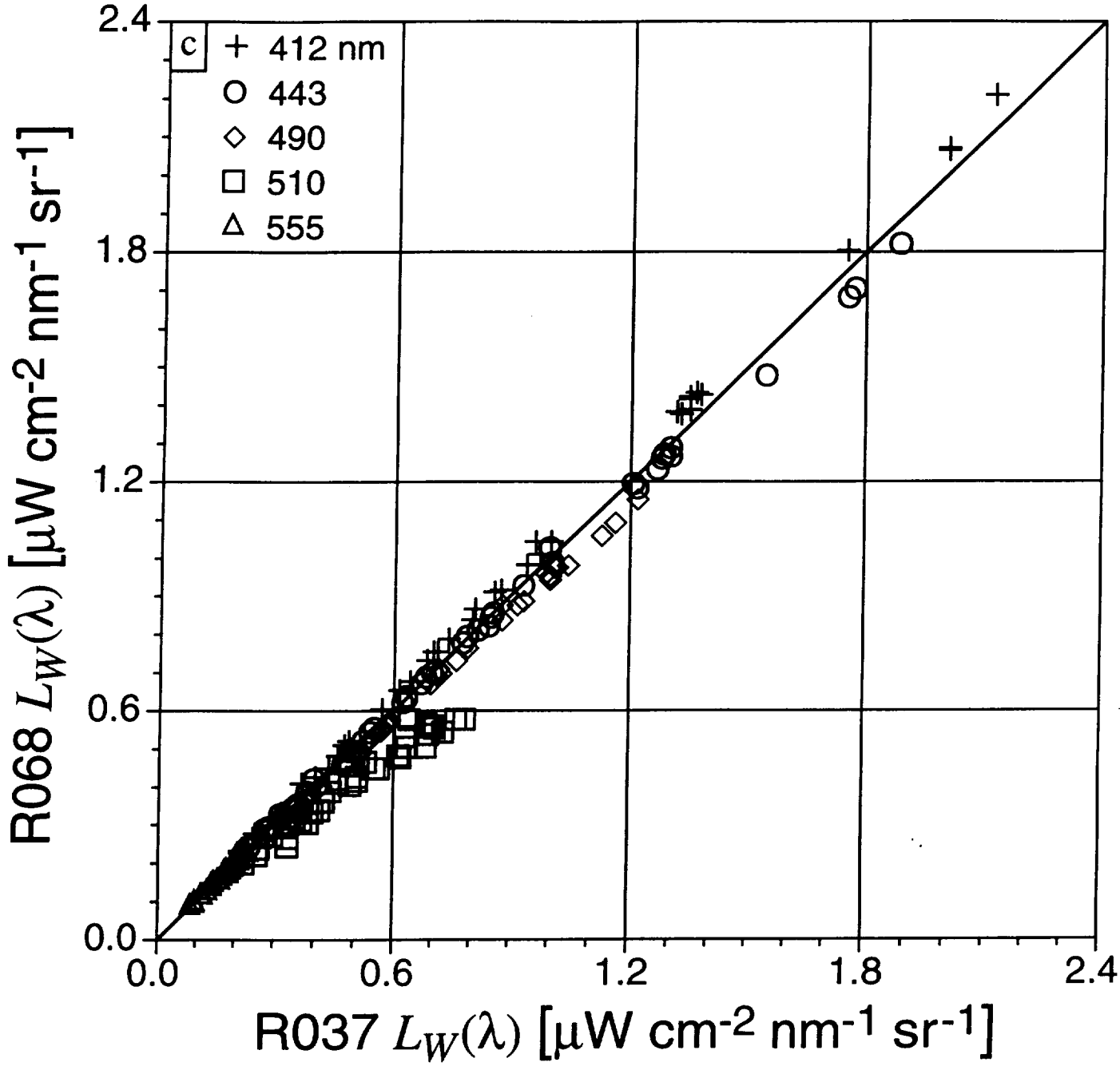
c
412 nm
443
490
510
555
2.4
1.8
1.2
0.6
0.0
0.0
0.6
1.2
1.8
2.4
R068 $L_W(\lambda)$ [µW cm^{-2} nm^{-1} sr^{-1}]
R037 $L_W(\lambda)$ [µW cm^{-2} nm^{-1} sr^{-1}]

Figure 5

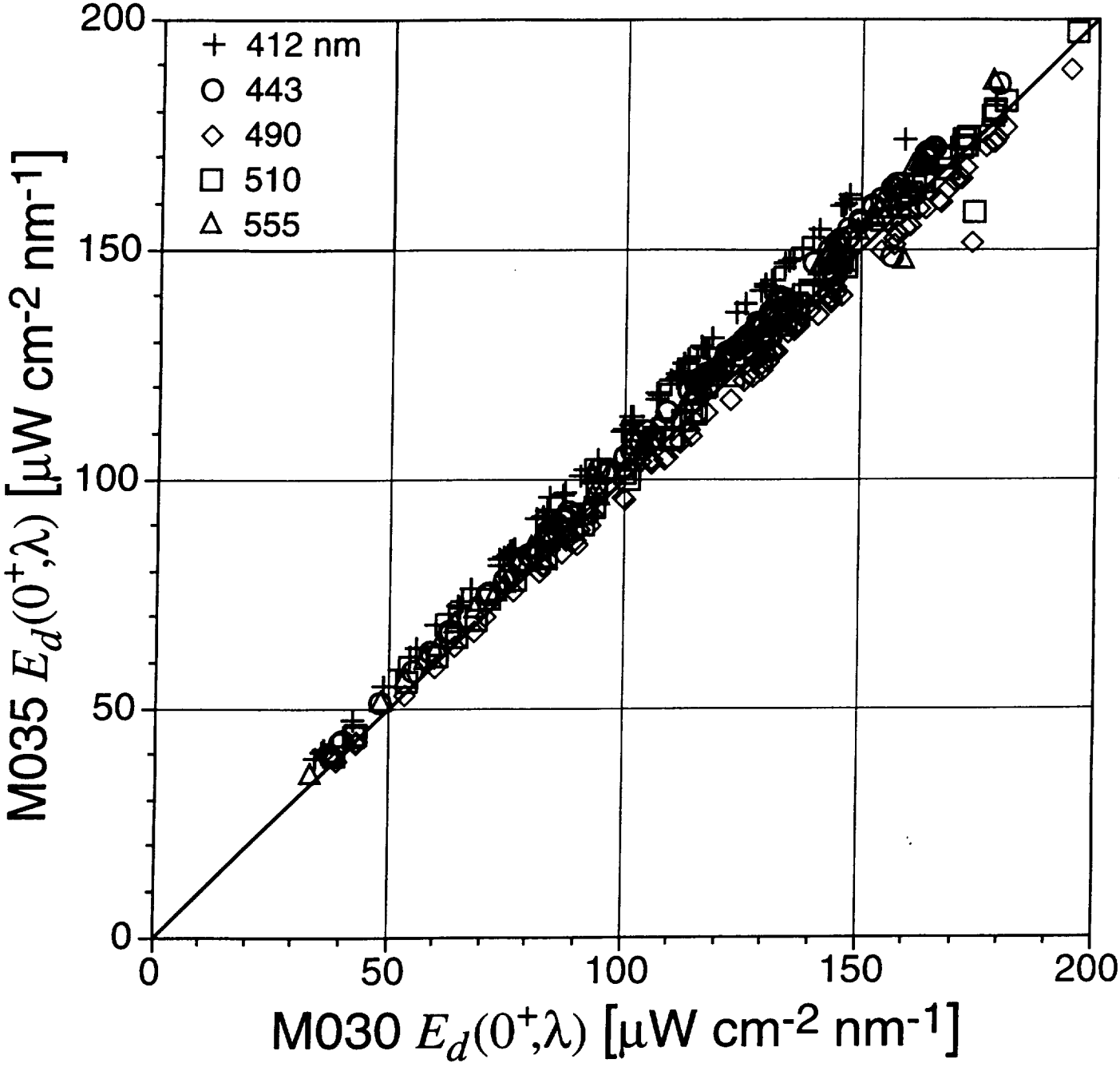
412 nm
443
490
510
555
200
150
100
50
0
0
50
100
150
200
M035 $E_d(0^+,\lambda)$ [μW cm^{-2} nm^{-1}]
M030 $E_d(0^+,\lambda)$ [μW cm^{-2} nm^{-1}]

Figure 6a

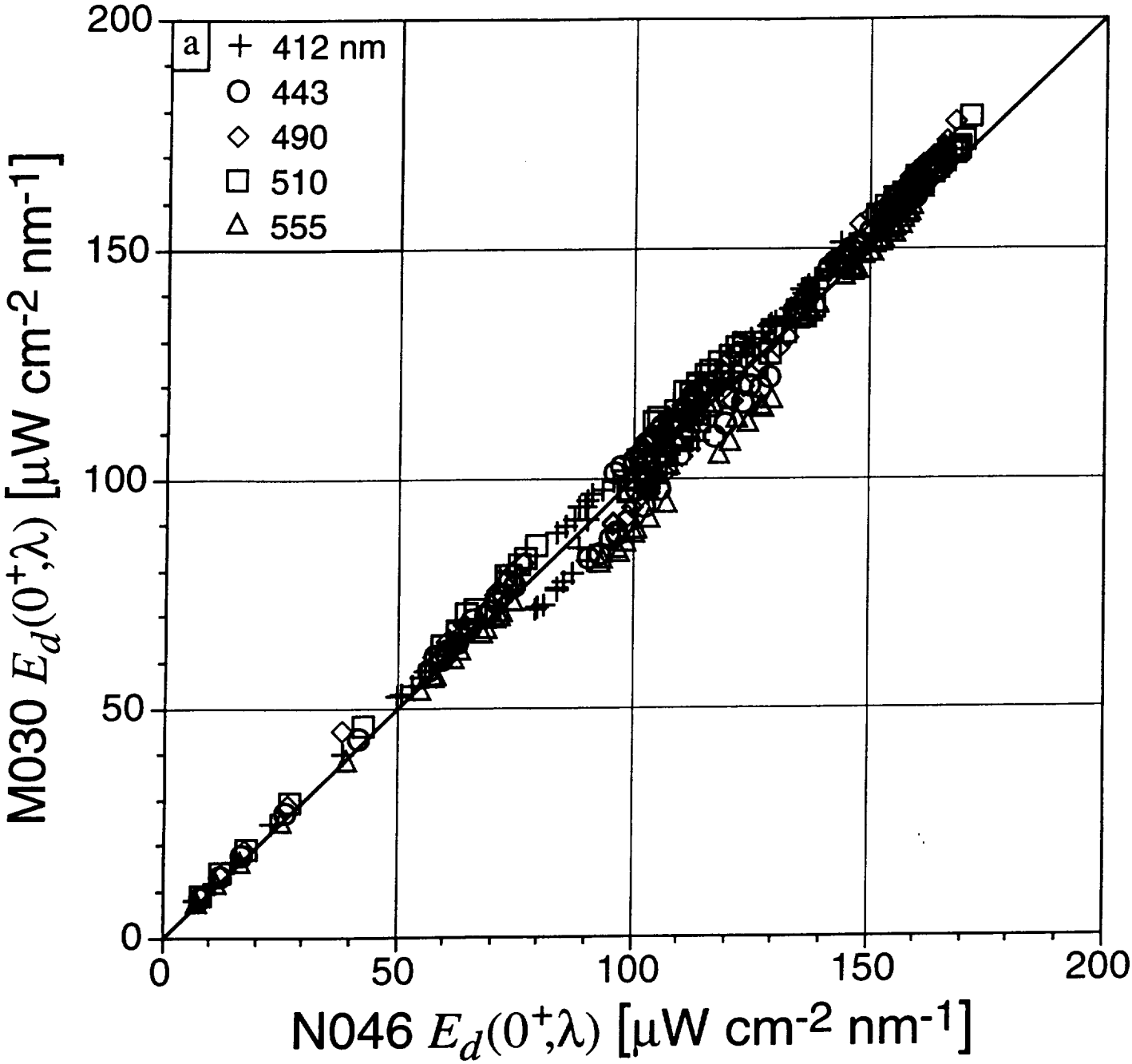
a
412 nm
443
490
510
555
200
150
100
50
0
0
50
100
150
200
M030 $E_d(0^+,\lambda)$ [μW cm^{-2} nm^{-1}]
N046 $E_d(0^+,\lambda)$ [μW cm^{-2} nm^{-1}]

Figure 6l

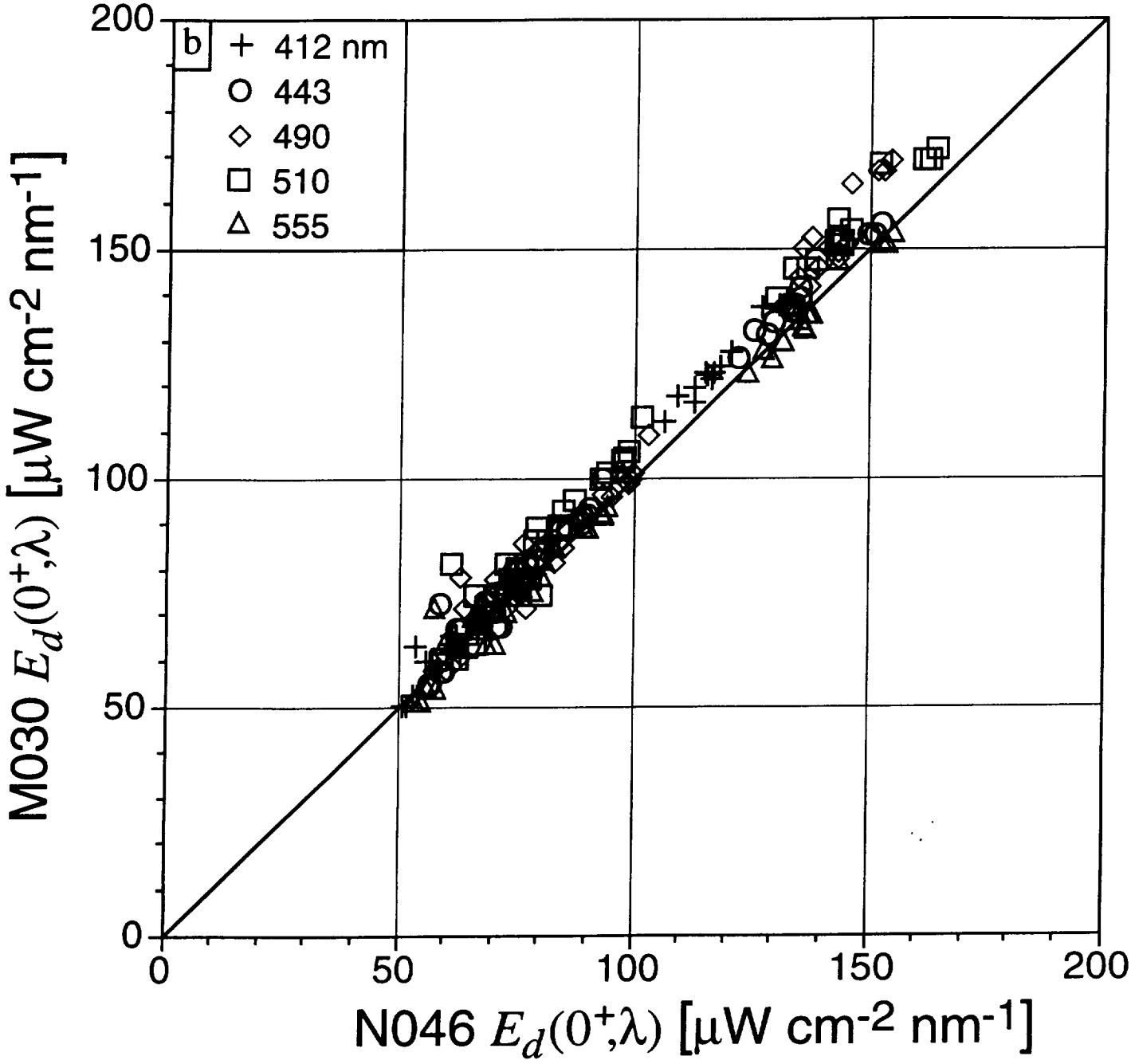
b
412 nm
443
490
510
555
200
150
100
50
0
0
50
100
150
200
M030 $E_d(0^+,\lambda)$ [μW cm^{-2} nm^{-1}]
N046 $E_d(0^+,\lambda)$ [μW cm^{-2} nm^{-1}]

Figure 7a

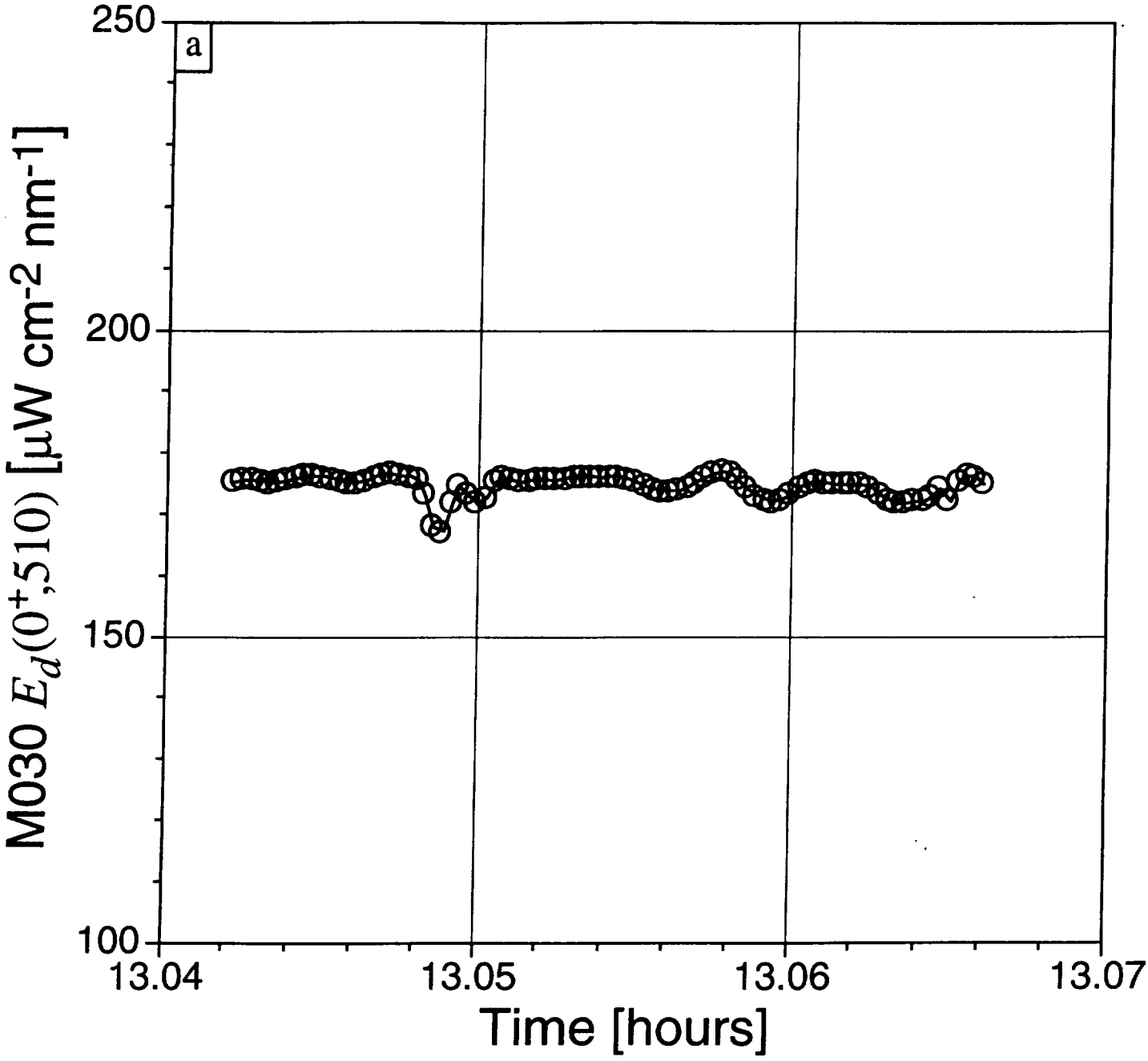
a
250
200
150
100
13.04
13.05
13.06
13.07
Time [hours]
M030 $E_d(0^+,510)$ [μW cm^{-2} nm^{-1}]

Figure 7b

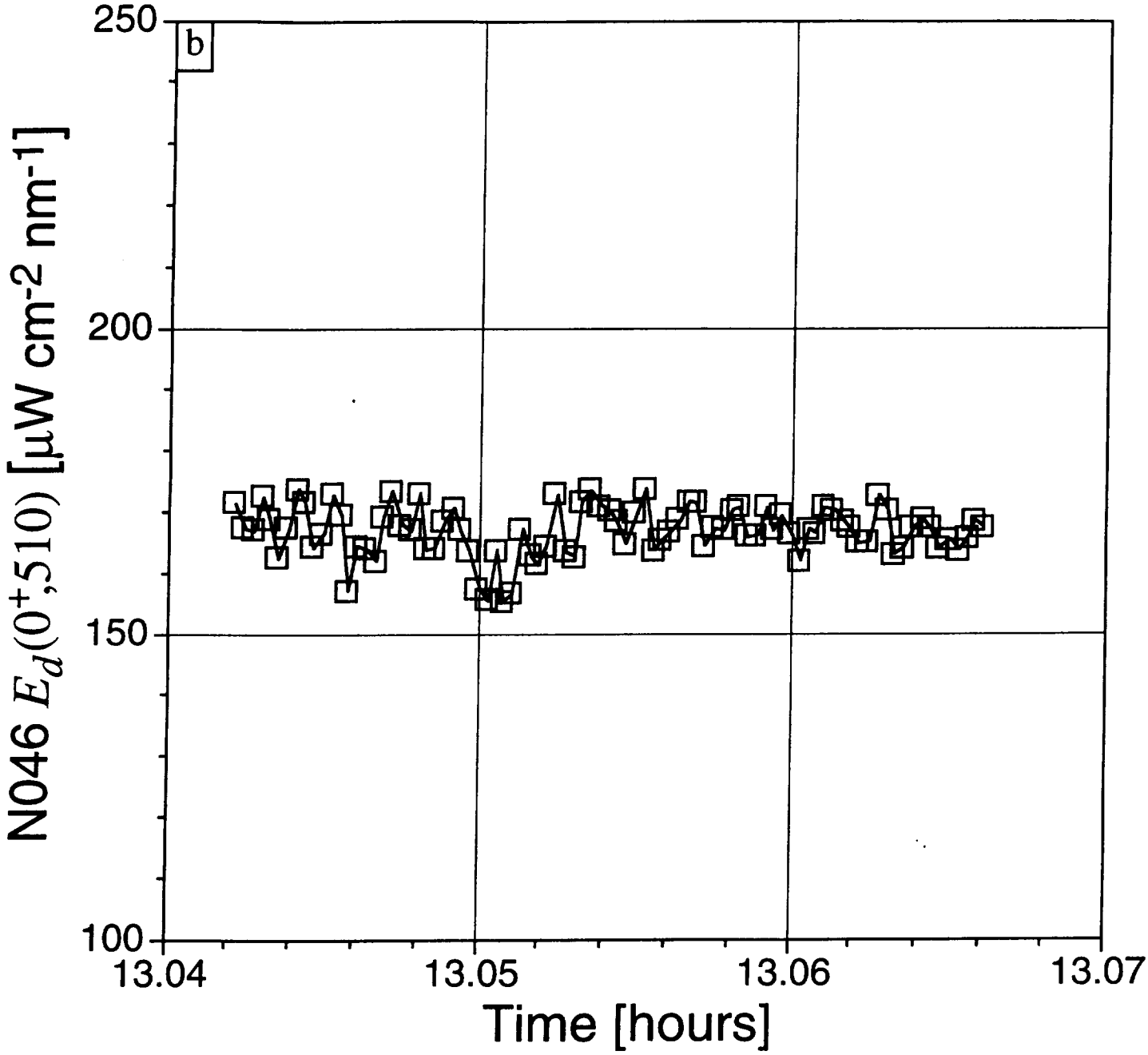
b
250
200
150
100
13.04
13.05
13.06
13.07
Time [hours]
N046 $E_d(0^+,510)$ [μW cm^{-2} nm^{-1}]

Figure 7c

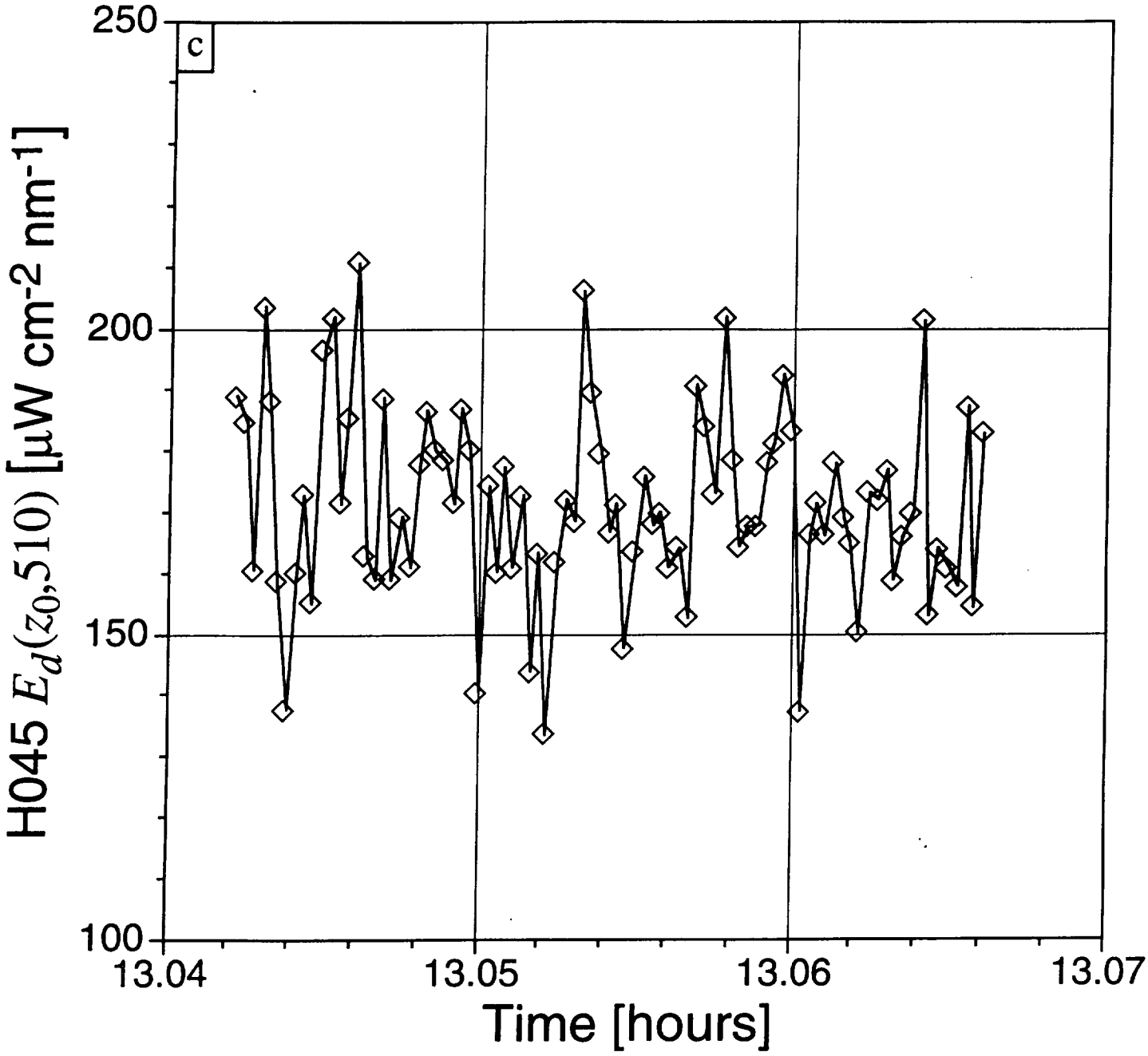
c
250
200
150
100
13.04
13.05
13.06
13.07
Time [hours]
H045 $E_d(z_0,510)$ [µW cm^{-2} nm^{-1}]

Figure 7c

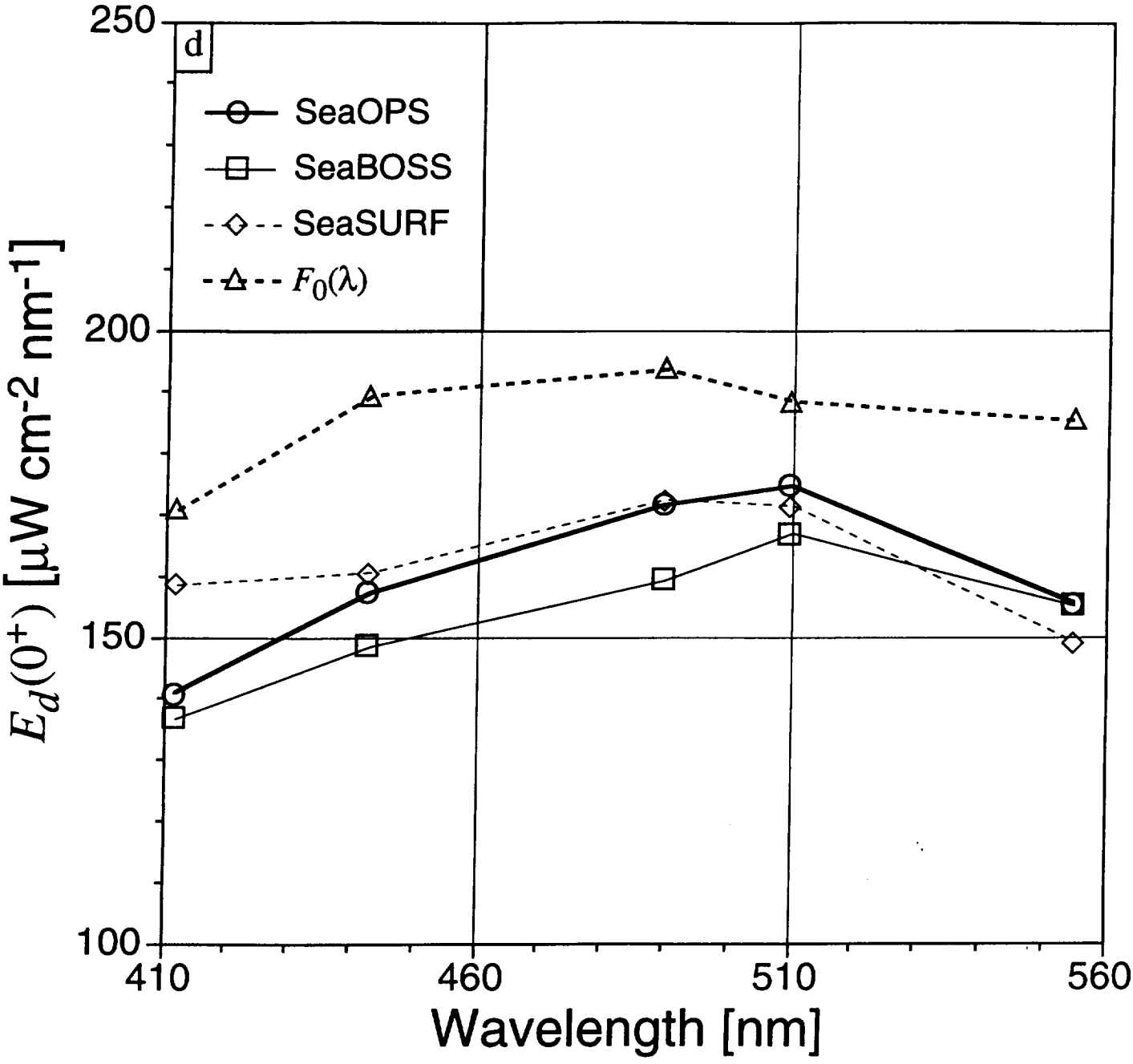
d
SeaOPS
SeaBOSS
SeaSURF
$F_0(\lambda)$
250
200
150
100
410
460
510
560
$E_d(0^+)$ [µW cm^{-2} nm^{-1}]
Wavelength [nm]

Figure 8a

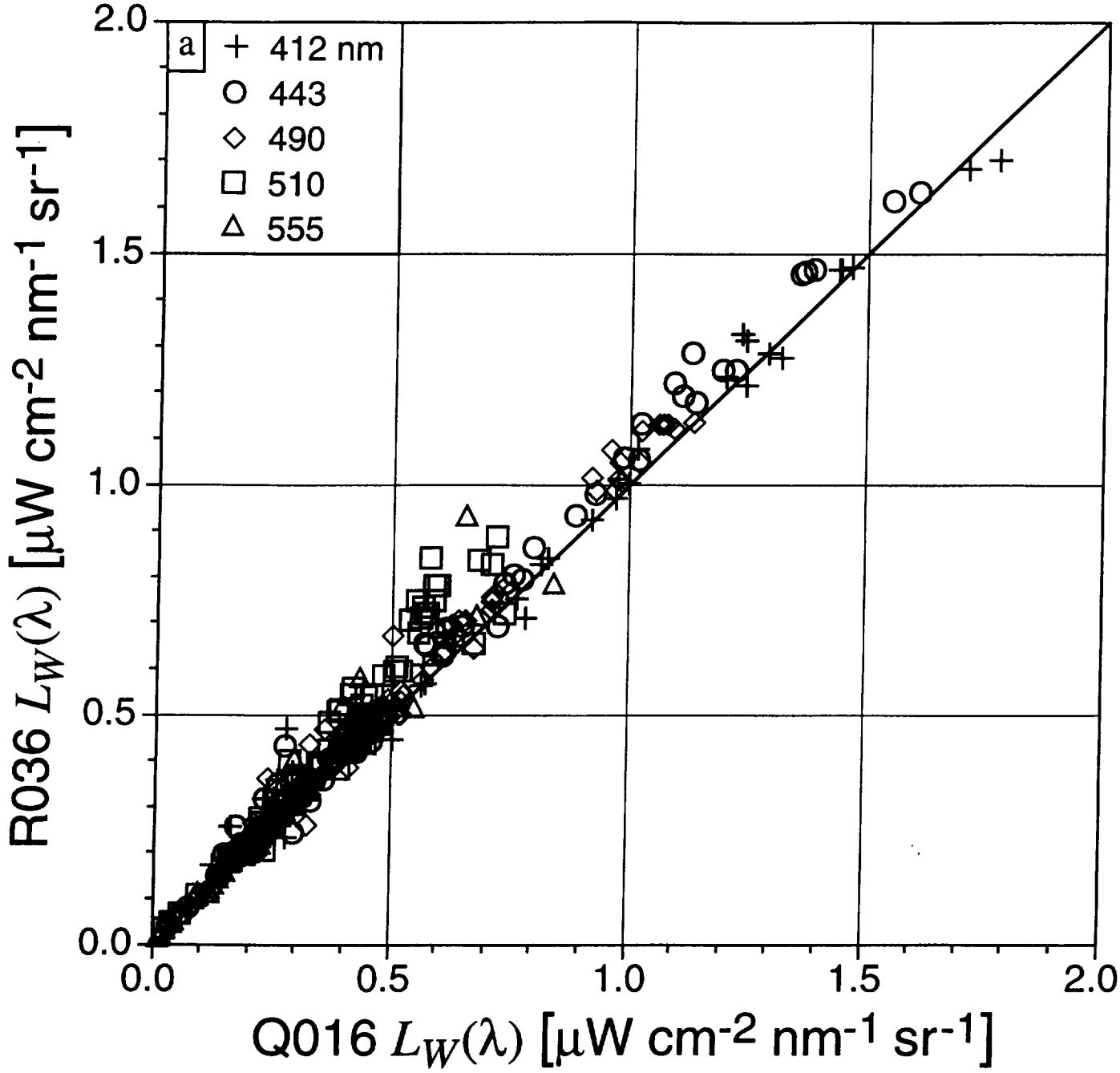
a
412 nm
443
490
510
555
2.0
1.5
1.0
0.5
0.0
0.0
0.5
1.0
1.5
2.0
R036 $L_W(\lambda)$ [µW cm^{-2} nm^{-1} sr^{-1}]
Q016 $L_W(\lambda)$ [µW cm^{-2} nm^{-1} sr^{-1}]

Figure 8l

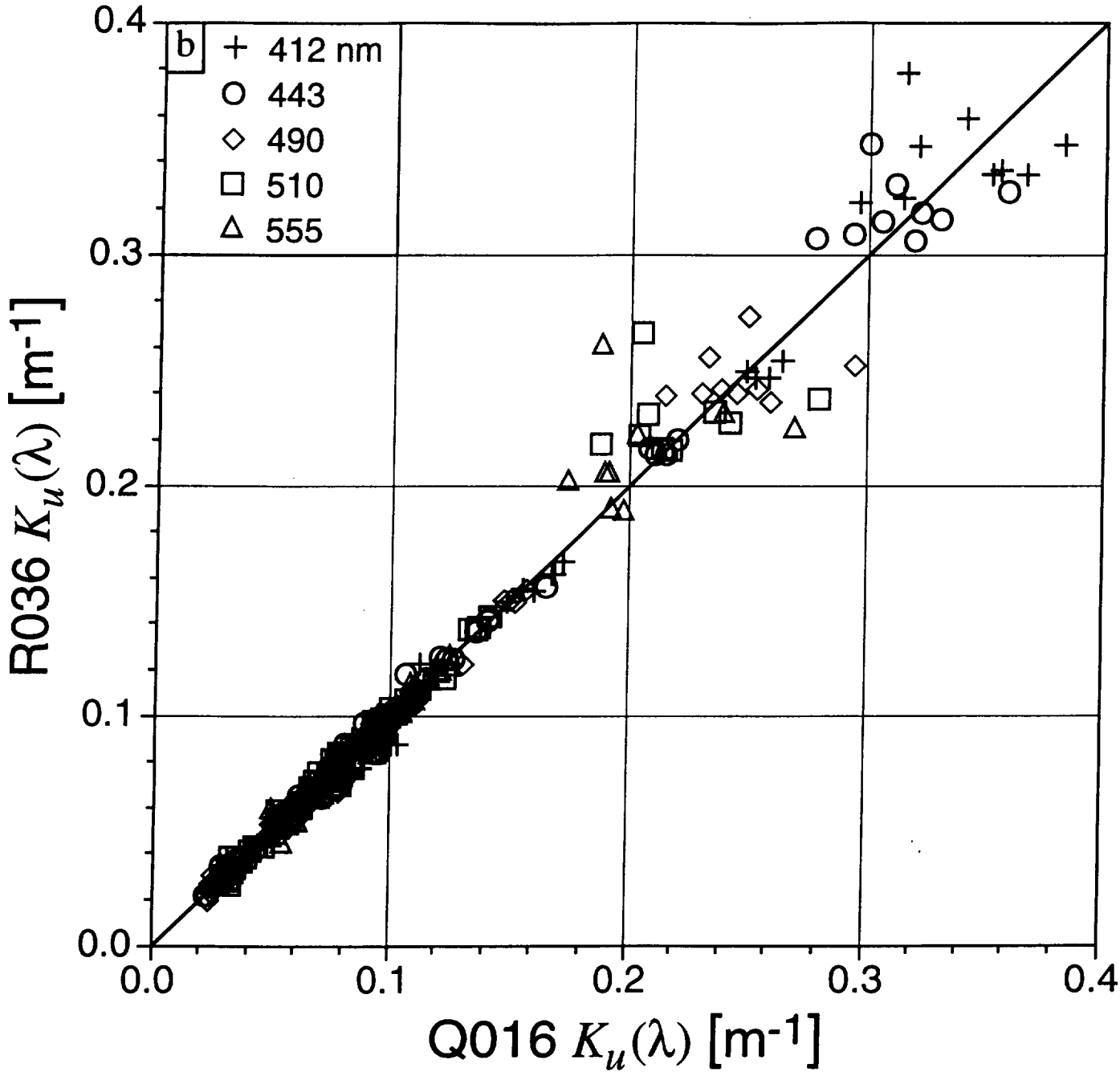
b
412 nm
443
490
510
555
0.0
0.1
0.2
0.3
0.4
R036 $K_u(\lambda)$ [m^{-1}]
Q016 $K_u(\lambda)$ [m^{-1}]

Figure 9:

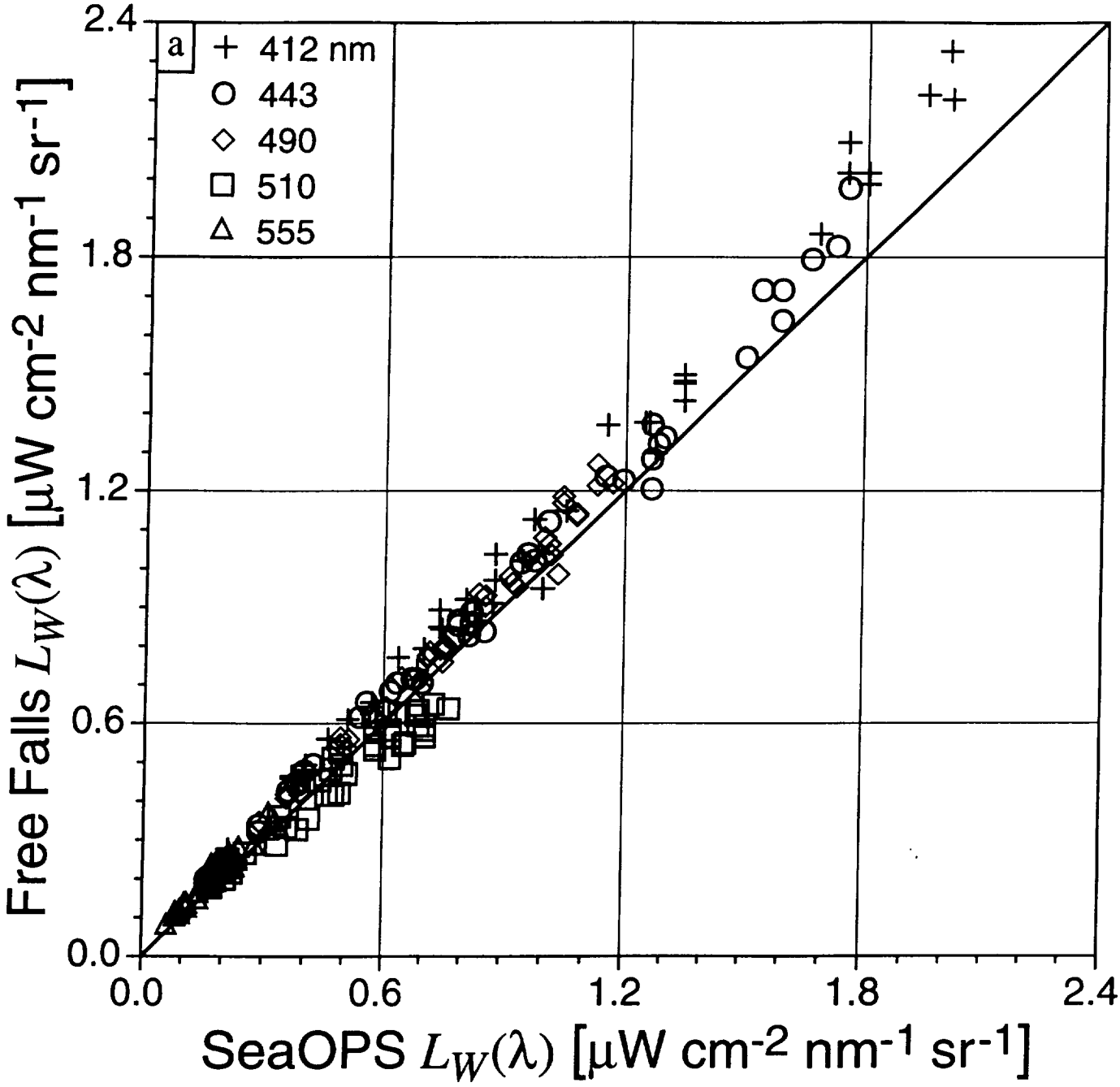
a
412 nm
443
490
510
555
2.4
1.8
1.2
0.6
0.0
0.0
0.6
1.2
1.8
2.4
Free Falls $L_W(\lambda)$ [μW cm^{-2} nm^{-1} sr^{-1}]
SeaOPS $L_W(\lambda)$ [μW cm^{-2} nm^{-1} sr^{-1}]

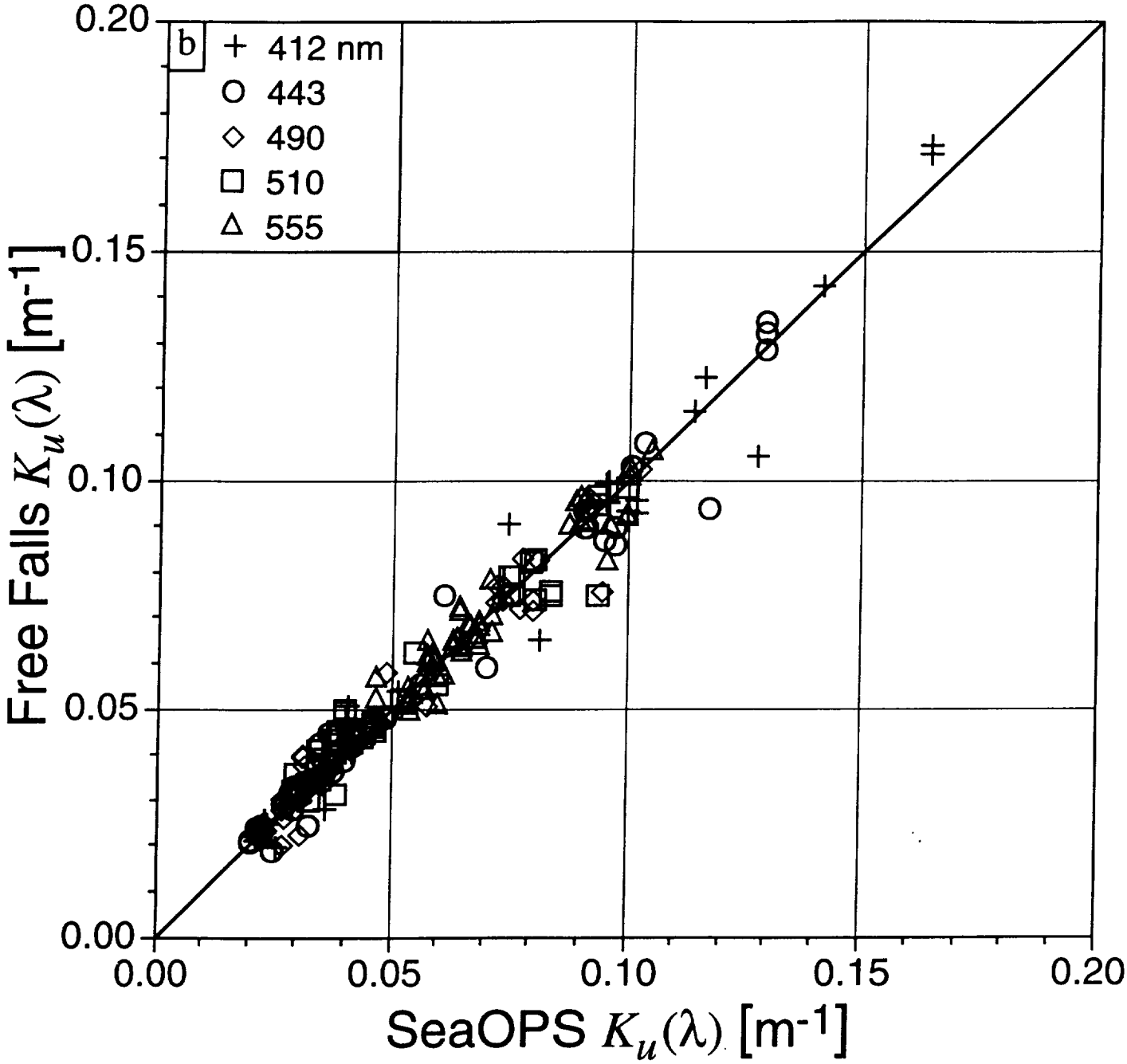
b
412 nm
443
490
510
555
0.20
0.15
0.10
0.05
0.00
0.00
0.05
0.10
0.15
0.20
Free Falls $K_u(\lambda)$ [m^{-1}]
SeaOPS $K_u(\lambda)$ [m^{-1}]